Control of detachment geometry on lateral variations in exhumation rates in the Himalaya: Insights from low-temperature thermochronology and numerical modeling

Xavier Robert,[1,2] Peter van der Beek,[1] Jean Braun,[1] Claire Perry,[1,2] and Jean-Louis Mugnier[3]

[1]   The Himalayan range is commonly presented as largely laterally uniform from west to east. However, geological structures, topography, precipitation rate, convergence rates, and low-temperature thermochronological ages all vary significantly along strike. Here, we focus on the interpretation of thermochronological data sets in terms of along-strike variations in geometry and kinematics of the main crustal detachment underlying the Himalaya: the Main Himalayan Thrust (MHT). We report new apatite fission track (AFT) ages collected along north-south transects in western and eastern central Nepal (at the latitudes of the Annapurna and Langtang massifs, respectively). AFT ages are consistently young (<3 Ma) along both N-S transects in the high-relief zone of the Higher Himalaya and increase (4 to 6 Ma) toward the south in the Lesser Himalaya. We compare our new data to published low-temperature thermochronological data sets for Nepal and the Bhutan Himalaya. We use the full data set to perform both forward and inverse thermal kinematic modeling with a modified version of the *Pecube* code in order to constrain potential along-strike variations in the kinematics of the Himalayan range. Our results show that lateral variations in the geometry of the MHT (in particular the presence or absence of a major crustal-scale ramp) strongly control the kinematics and exhumation history of the orogen.

1.   Introduction

[2]   The high elevation of active convergent mountain belts is driven by a balance between tectonic processes that build topography and erosional processes that lower it. The system is dynamic, with feedbacks that would tend to drive orogenic systems toward steady state [*Adams*, 1980; *Jamieson and Beaumont*, 1988; *Willett and Brandon*, 2002]. Because of its rapid convergence and exhumation rates, the Himalayan orogen provides an excellent natural laboratory to study evolving orogenic systems and mountain building processes. Numerous balanced geological cross sections have been constructed to infer the geological structure of the Himalaya and to develop scenarios for its kinematic development [e.g., *Schelling and Arita*, 1991; *Srivastava and Mitra*, 1994; *DeCelles et al.*, 2001; *Pearson and DeCelles*, 2005;

Robinson et al., 2006; *McQuarrie et al.*, 2008] and its deep structure is known through several geophysical experiments [e.g., *Hirn and Sapin*, 1984; *Zhao et al.*, 1993; *Schulte-Pelkum et al.*, 2005; *Nabelek et al.*, 2009]. During the last twenty years, thermochronological data sets have been published that constrain exhumation rates and pathways along several transects across the range [e.g., *Copeland et al.*, 1991; *Catlos et al.*, 2001; *Bollinger et al.*, 2004; *Thiede et al.*, 2004; *Vannay et al.*, 2004; *Grujic et al.*, 2006; *Blythe et al.*, 2007].

[3]   The structure of the Himalayan orogen (Figure 1) is classically considered as showing little lateral variation from west to east. The orogen is built by a north dipping, southward propagating, crustal-scale thrust sequence [*Gansser*, 1964; *Le Fort*, 1975; *Hodges*, 2000] (cf. *Yin* [2006] for a recent review). However, several authors have invoked potential out-of-sequence reactivation of the more internal part of the belt [*Brunel and Andrieux*, 1980; *Harrison et al.*, 1998; *Hodges et al.*, 2004; *Wobus et al.*, 2005], possibly climatically controlled through rapid and focused recent erosion [*Thiede et al.*, 2004; *Hodges et al.*, 2004].

[4]   In contrast to the popular two-dimensional cross section view of the Himalaya, topography and relief [*Duncan et al.*, 2003; *Bookhagen and Burbank*, 2006], precipitation rates and patterns [*Bookhagen et al.*, 2005; *Bookhagen and Burbank*, 2006; *Grujic et al.*, 2006], orogen

---

[1]Institut des Sciences de la Terre, Université Joseph Fourier, CNRS, Grenoble, France.
[2]GEOTOP, Département des Sciences de la Terre et de L'atmosphère, Université du Québec à Montréal, Montreal, Québec, Canada.
[3]Institut des Sciences de la Terre, CNRS, Université de Savoie, Le Bourget-du-Lac, France.
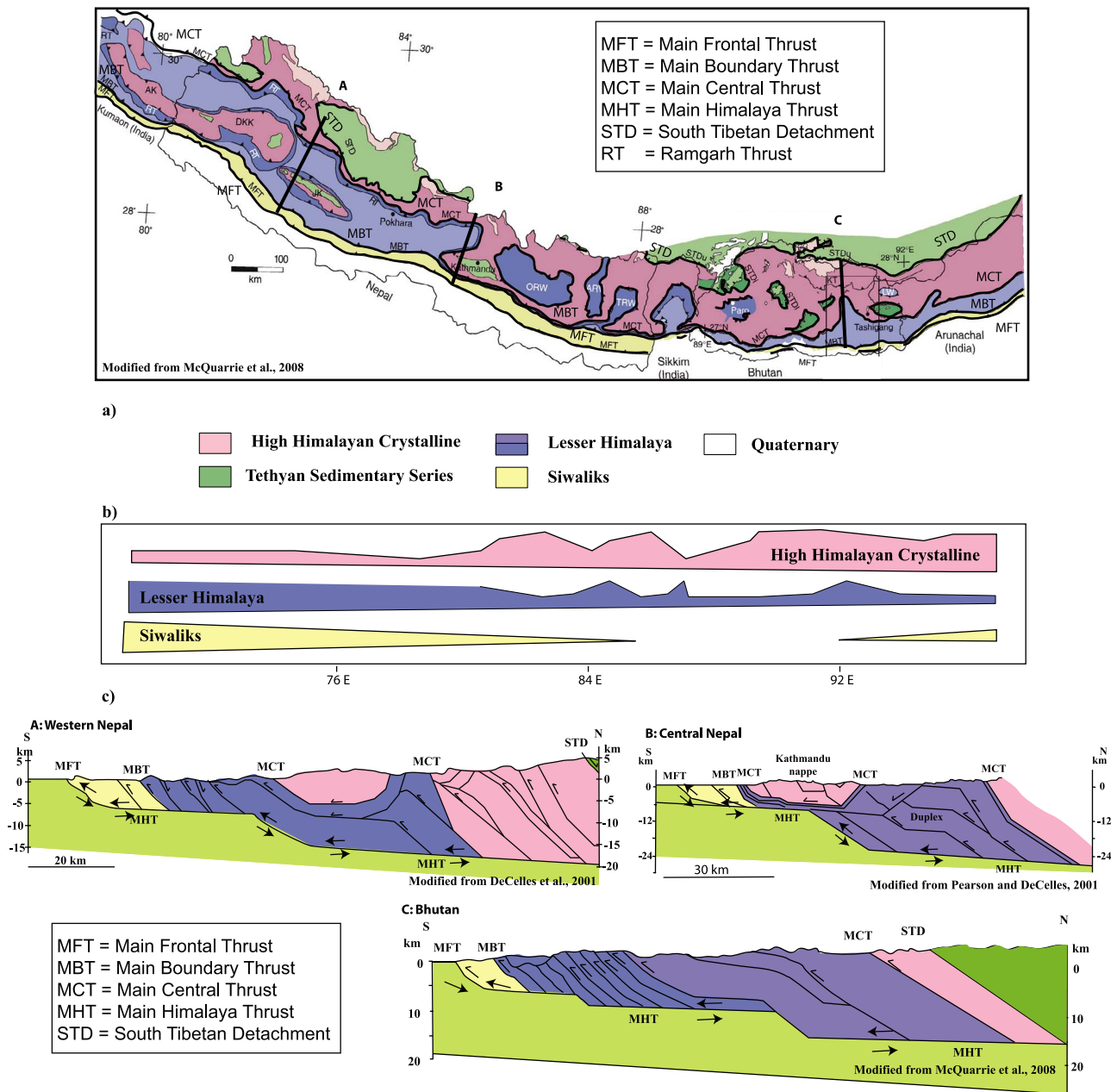
Figure 1. (a) Simplified geological map of the Himalaya showing the major structural units and the major thrusts [modified from *McQuarrie et al.*, 2008 with permission from Elsevier]; lines indicate locations of three structural cross sections shown in Figure 1c. (b) Schematic representation of the relative widths of the High Himalayan crystalline, Lesser Himalaya, and Siwaliks along strike of the Himalaya. (c) Structural cross sections across western Nepal (cross section A) [modified from *DeCelles et al.*, 2001], central Nepal (cross section B) [modified from *Pearson and DeCelles*, 2005], and the Bhutan Himalaya (cross section C) [modified from *McQuarrie et al.*, 2008]. Color scheme in cross sections is same as in map.

structure [*Yin*, 2006], and convergence rates [*Larson et al.*, 1999; *Paul et al.*, 2001] all vary significantly from west to east, showing that the Himalayan range is not laterally uniform when studied in a minimum of detail. Whether climatic parameters, tectonic forcing or preexisting structures control these lateral variations remains a difficult question to answer, due to the coupled nature of these potential forcing parameters. Topography drives variations in climate and erosion rates [*Montgomery and Brandon*, 2002; *Roe*, 2005], and tectonics drive topography. Erosion rate depends on relief, elevation, lithology and rainfall [e.g., *Summerfield and Hulton*, 1994; *Hovius*, 1998; *Burbank*, 2002] and influences topography and tectonics [*Willett*, 1999; *Stolar et al.*, 2007]. A better understanding of the lateral spatial variations in kinematics and exhumation rates is thus required to resolve the fundamental controls on topography and erosion in the Himalaya, and may also provide more general insight into the coupling mechanisms

between crustal-scale geometry, orogen kinematics, climate and erosion.

[5] To address these issues, we employ both forward and inverse numerical modeling, using a newly developed thermokinematic model to explain observed patterns of low-temperature thermochronological ages (mainly apatite fission track; AFT) along three transects across western central Nepal, eastern central Nepal and Bhutan. The upper crustal thermal structure is strongly affected by orogen kinematics, fault geometry and surface processes that shape the landscape and control the wavelength of topography [e.g., *Ehlers*, 2005; *Braun et al.*, 2006; *Reiners and Brandon*, 2006]; which are thus recorded by the time-temperature-depth history of exhumed rocks. In optimal conditions, low-temperature thermochronometry (using multiple thermochronometers or systems that record the integrated temperature history such as fission track lengths or noble gas age spectra) constrains the temperature field and rock exhumation paths through its record of the time-temperature history. However, in a highly complex and dynamic system such as the Himalayan orogen, characterized by spatial and temporal variability in rock advection rates, nonvertical particle paths controlled by the geometry of major faults, and a strong influence of topography on the upper crustal thermal structure, numerical models are essential to extract meaningful information from thermochronologic data [*Braun et al.*, 2006].

[6] In the following, we first review the geologic structure, kinematics, topography and climate of the central and eastern Himalaya, including a discussion of recent controversies about the thrust sequence and lateral variations in structure. We then present the AFT data, combining our own data with published data sets, and the numerical model that forms the basis for this study. We use synthetic data to test the resolution of our model, and show inverse model results that constrain the crustal geometry and kinematics along the three studied transects.

[7] For the transect in central Nepal, where the recent kinematics of the belt have been strongly disputed in recent years [*Avouac*, 2003; *Bollinger et al.*, 2004; *Hodges et al.*, 2004; *Bollinger et al.*, 2006; *Wobus et al.*, 2006], we demonstrate that existing low-temperature thermochronology data do not have sufficient resolution to discriminate between different kinematic models for the Quaternary evolution of the belt. They do, however, rule out initiation of out-of-sequence thrusting before the Quaternary and highlight particular kinematic and thermal conditions implied by this model. They also constrain the geometry of the crustal-scale detachment underlying the orogen; the Main Himalayan Thrust [*Hirn and Sapin*, 1984; *Zhao et al.*, 1993; *Makovsky et al.*, 1996; *Schulte-Pelkum et al.*, 2005]. Results from the other two transects highlight important along-strike variations in this geometry, which are shown to exert a first-order control on exhumation rates. From this synthesis of exhumation patterns in the Himalayan orogen, we propose a geometric and kinematic model for its recent evolution.

2. Tectonic and Morphologic Setting

2.1. Geological Structure of the Himalaya

[8] The Himalayan orogen is characterized by a series of north dipping crustal-scale faults that delimit four distinct tectonic units [*Le Fort*, 1975; *Hodges*, 2000; *Yin and Harrison*, 2000], which can be followed along its 2500 km length (Figure 1a). The northernmost Tethyan Himalayan zone consists of Cambrian to Eocene sedimentary to low-grade metamorphic rocks. It is separated from the structurally underlying higher (or greater) Himalaya by the dominantly extensional South Tibetan Detachment System (STDS) [*Burchfiel et al.*, 1992]. The Higher Himalaya crystalline thrust sheet consists of high-grade metamorphic rocks, with abundant evidence for partial melting, and overthrusts the Lesser Himalaya along the Main Central Thrust (MCT). Precise dating of the activity of the STDS and MCT has shown that they were active simultaneously during the Early Miocene (around 22–18 Ma) [*Burchfiel et al.*, 1992; *Hodges et al.*, 1996], giving rise to the "channel flow" model of extrusion of partially molten Higher Himalayan middle crust from under the overthickened Tibetan Plateau [*Nelson et al.*, 1996; *Beaumont et al.*, 2001; *Hodges et al.*, 2001; *Grujic et al.*, 2002].

[9] The Lesser Himalaya forms a complex structural duplex with several major internal thrusts [*Schelling and Arita*, 1991; *DeCelles et al.*, 2001]. In Nepal, these indicate a forward propagating sequence that initiated after cessation of activity on the MCT. Thrusts in the internal Lesser Himalaya of western Nepal were active between ~12 and 15 Ma [*DeCelles et al.*, 2001; *Robinson et al.*, 2006] and the Lesser Himalayan duplex was built since ~12–10 Ma [*DeCelles et al.*, 2001; *Huyghe et al.*, 2001; *Robinson et al.*, 2006]. The Lesser Himalaya varies strongly in width along strike, due to the presence or absence of a lid of Higher Himalayan rocks that have overthrusted the Lesser Himalaya up to 150 km southward of the general trace of the MCT (Figure 1). The Higher Himalayan rocks form a series of prominent klippen in Nepal [*Schelling and Arita*, 1991; *Upreti and Le Fort*, 1999; *DeCelles et al.*, 2001]. In the eastern Himalaya, Lesser Himalayan tectonic structures are similar, but the unit has been reduced to a narrow width and has been strongly deformed in the Bhutan Himalaya [*Gansser*, 1983; *Bhargava*, 1995; *Grujic et al.*, 2002; *McQuarrie et al.*, 2008].

[10] The Lesser Himalaya overthrusts the sub-Himalaya or Siwalik thrust belt, composed of Miocene-Pliocene syntectonic clastic deposits, along the Main Boundary Thrust (MBT). In the western and central Himalaya, the MBT was active from 11 Ma to ~5 Ma [*Meigs et al.*, 1995; *DeCelles et al.*, 2001]. The Siwaliks form a wide and structurally complex zone in the western Himalaya [e.g., *Powers et al.*, 1998; *Mugnier et al.*, 1999], but are composed of a single discontinuous thrust sheet of narrow width in Bhutan [*Gansser*, 1983; *Lakshminarayana and Singh*, 1995]. The Siwaliks overthrust the Ganges plain along the currently active Main Frontal Thrust (MFT) [*Lavé and Avouac*, 2001].

[11] Geophysical and structural studies suggest that all the major thrusts in the Himalaya, including the MFT, MBT and MCT, branch at depth from a single major midcrustal décollement, the Main Himalayan Thrust (MHT) [*Hirn and Sapin*, 1984; *Zhao et al.*, 1993; *Makovsky et al.*, 1996; *Avouac*, 2003; *Schulte-Pelkum et al.*, 2005, *Nabelek et al.*, 2009] (Figure 1c). In Nepal, where it is best studied, geophysical and structural data show that the MHT is characterized by a ramp-and-flat geometry with two major ramps. The frontal ramp is shallow and corresponds to the position of the emerging MFT, with a dip angle around 30° at the
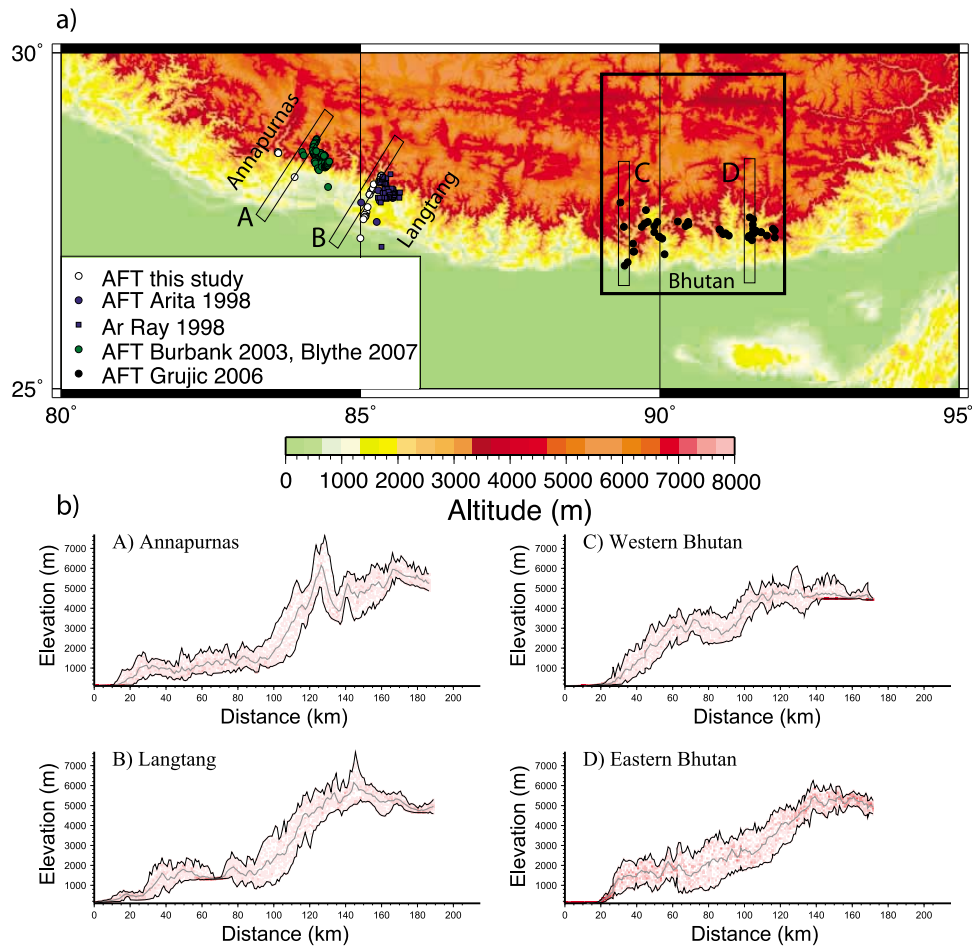
Figure 2. (a) DEM of the central and eastern Himalaya showing the location of studied transects and thermochronological data used in this study. Transect A corresponds to the Annapurna-Buthwal region; transect B corresponds to the Langtang-Hetauda region; transects C and D correspond to the Western and Eastern Bhutan Himalaya, respectively. (b) Swath elevation profiles for each transect. Black solid line corresponds to the mean elevation calculated in the corresponding 20 km wide box; outer gray lines correspond to the maximum and minimum elevations, and the red fill corresponds to the probability density of elevation within the envelope.

surface. The other ramp is believed to occur at midcrustal depth beneath the sharp topographic front of the high range [*Avouac*, 2003]. Geophysical data from central Nepal [*Lemonnier et al.*, 1999; *Pandey et al.*, 1999; *Nabelek et al.*, 2009] suggest a dip angle of ~10° to 15° for the midcrustal ramp; mechanical modeling based on the present-day displacement field measured by GPS surveys [*Berger et al.*, 2004] suggests a somewhat higher dip of ~30°.

[12] From a detailed analysis of GPS data, *Berger et al.* [2004] have proposed that the MHT is segmented and the crustal ramp more pronounced in central Nepal than in western Nepal, in accord with balanced structural cross sections based on surface geology [*DeCelles et al.*, 2001; *Mugnier et al.*, 2004]. Similarly, drainage patterns [*van der Beek et al.*, 2002] and present-day displacement rates [*Larson et al.*, 1999] suggest that the southern, shallow flat segment is steeper in western Nepal than in central Nepal. In Bhutan, the deep fault structure is poorly known because of a lack of geophysical studies. *Hauck et al.* [1998] present

a crustal transect from deep reflection seismic profiling of the Himalayan orogen at ~90 °E. Combined with published geological cross sections, they suggest a major lateral change in geometry to occur along the "Yadong cross structure" [*Burchfiel et al.*, 1992], which underlies a major left-lateral offset in the main Himalayan structures and topography roughly along the Sikkim-Bhutan border. To the west of this structure, the MHT shows a crustal ramp underlying the MCT zone, similar to central Nepal, whereas to the east, the MHT appears to dip more shallowly and contains a crustal ramp much further to the north, underneath the Tethyan Himalayan zone.

2.2. Topographic and Climatic Variability

[13] The topography of the Himalaya varies strongly along strike [*Duncan et al.*, 2003; *Bookhagen and Burbank*, 2006]. Figure 2 presents a digital elevation model (DEM) and elevation profiles through Nepal and Bhutan perpendicular to the major structures, constructed from Shuttle

Radar Topography Mission (SRTM) data. In both Nepal and Bhutan, the distance from the deformation front (MFT), with elevations near sea level, to the range crest, with elevations >7000 m, is 130–150 km. Topographic profiles in central Nepal are strongly concave; the mean topography in the Lesser Himalaya rises to only 2000 m at ~100 km north of the MFT, before rising to close to 7000 m in the next 30–50 km. There thus exists a sharp physiographic transition 10 to 30 km south of the MCT in central Nepal [*Seeber and Gornitz*, 1983; *Lavé and Avouac*, 2001; *Duncan et al.*, 2003; *Wobus et al.*, 2003], which is situated above the deep crustal ramp of the MHT. This physiographic transition has been interpreted in different ways, related to the kinematic models proposed for the central Himalaya [*Lavé and Avouac*, 2001; *Avouac*, 2003; *Wobus et al.*, 2003, 2005; *Bollinger et al.*, 2004; *Hodges et al.*, 2004] (see discussion in section 2.3).

[14] As previously shown by *Duncan et al.* [2003] and *Bookhagen and Burbank* [2006], the morphology is very different in the eastern (Bhutan) Himalaya, where the topography shows an almost straight to slightly convex taper. Consequently, the topography rises more steeply from the deformation front and the 2000 m elevation contour is reached within 50 km from the front, whereas the rise to the high peaks is much more gradual than in Nepal.

[15] *Bookhagen and Burbank* [2006] combine their topographic analysis with satellite precipitation data (TRMM) to show two distinct precipitation maxima along strike in the Himalaya. An outer, continuous band occurs along the southern edge of the Lesser Himalaya, where elevations reach ~1000 m. A second band occurs where the physiographic transition from the Lesser to the Higher Himalaya exists and is thus discontinuous along strike, disappearing to the east. Previous studies have revealed two more general Himalayan precipitation gradients: a strong orographic gradient across the belt, with precipitation decreasing from over 3000 mm y^{-1} (and locally up to 10,000 mm y^{-1}) on the southern flank to <200 mm y^{-1} on the Tibetan Plateau [*Roe*, 2005; *Anders et al.*, 2006], as well as an overall east-west decrease in precipitation [*Bookhagen et al.*, 2005], due to the fact that the major moisture source for monsoon precipitation, the Bay of Bengal, lies to the southeast of the Himalayan belt.

2.3. Kinematics of the Himalaya

[16] GPS measurements [*Bilham et al.*, 1997; *Larson et al.*, 1999; *Jouanne et al.*, 2004] constrain present-day convergence rates across the central Himalaya to 18 ± 3 mm y^{-1}. They show a west-to-east increase in convergence rate, consistent with the location of the India-Eurasia rotation pole to the west of the collision zone [*Larson et al.*, 1999; *Paul et al.*, 2001]. The present-day rates are similar to Holocene shortening rates across the MFT in Nepal of 14–21 km My^{-1}, from folded and uplifted river terraces [*Lavé and Avouac*, 2000; *Mugnier et al.*, 2004], as well as to Quaternary shortening rate across the Siwaliks (~19 km My^{-1}) [*Mugnier et al.*, 2004] and Miocene-Pliocene shortening rates across the Lesser Himalaya (19–22 km My^{-1}) [*DeCelles et al.*, 2001]. The similarity of rates on different timescales suggests that the Himalayan orogen has absorbed part of the India-Eurasia convergence and propagated toward the Indian continent at constant rates since mid-Miocene times (15–20 Ma) [*Mugnier and Huyghe*, 2006].

[17] In a reference frame attached to the MHT, this convergence is partitioned into underthrusting of the Indian plate and overthrusting of the Himalayan orogen (compare X. Robert et al., Kinematic models of the central Himalaya: A critical evaluation, submitted to *Earth Science Reviews*, 2011, for a more detailed discussion). Several authors [*Bollinger et al.*, 2006; *Brewer and Burbank*, 2006; *Whipp et al.*, 2007] have shown that available thermochronological data for central Nepal limit overthrusting velocities to 5–6 km My^{-1} since ~10 Ma, implying underthrusting of India (or underplating and forward propagation of the Himalayan thrust wedge) at a rate of ~15 km My^{-1} since that time.

[18] Recently, two competing models have been proposed to describe the present-day kinematics of the central Nepal Himalaya and explain the sharp physiographic transition. These differ principally in their predictions of which surface-breaking faults accommodate current shortening and what kinematics drive rapid exhumation in the topographic transition zone around the MCT. *Avouac* [2003] and *Bollinger et al.* [2004, 2006] argue that recent deformation is concentrated along the MHT, generating major (M > 8) earthquakes on this thrust, and that rapid exhumation in the MCT zone results from combined underplating and overthrusting along the MHT ramp. In contrast, *Wobus et al.* [2003] and *Hodges et al.* [2004] suggest active Quaternary out-of-sequence thrusting in the MCT zone, possibly driven by strongly localized climatically controlled exhumation in this area. A jump in detrital thermochronologic and cosmogenic radionuclide ages across the topographic transition in central Nepal has been argued to support the latter model [*Wobus et al.*, 2003, 2005, 2006].

3. Thermochronology Data

3.1. Existing Data Sets and Sampling Strategy

[19] We use new apatite fission track (AFT) and existing AFT and mica Ar-Ar ages, together with numerical modeling to constrain the geometry and kinematics of major faults along three north-south transects through the central and eastern Himalaya. A major obstacle to obtaining thermochronologic data sets across the entire Himalayan orogen lies in the unfavorable lithologies of the Lesser Himalaya, which consist mainly of fine-grained pelitic rocks with low degrees of metamorphism. We have chosen three areas where it is either possible to obtain AFT data or where extensive low-temperature thermochronologic data already exist. These are, from west to east (Figure 2a): the Annapurna region in west central Nepal, the Langtang-Kathmandu region in east central Nepal, and the Bhutan Himalaya.

[20] We have collected samples for AFT thermochronometry along two transects across the range. In a previous study, we presented data from the MCT zone along the Trisuli River (Langtang Himal) across the Kathmandu klippe to the MBT at Hetauda in east central Nepal [*Robert et al.*, 2009]. Here, we complete these with a transect collected in west central Nepal, from the MCT zone along the Kali Gandaki valley (Annapurna massif) to the MBT at Buthwal. We concentrated our sampling on the Lesser Himalaya since the vast majority of existing data was collected in the Higher Himalaya. Our sampling strategy aimed at obtaining transects from the MBT northward to and

Table 1. Apatite Fission Track Data From Central Nepal[a]

Sample	Elevation (m)	N	ρ_s ($\times 10^6$ cm^{-2})	N_s ($\times 10^6$ cm^{-2})	ρ_i ($\times 10^6$ cm^{-2})	N_i ($\times 10^6$ cm^{-2})	ρ_d ($\times 10^6$ cm^{-2})	N_d ($\times 10^6$ cm^{-2})	P(χ^2) (%)	D (%)	Age (Ma)	$\pm 1\sigma$ (Ma)
NP05.06	650	21	3.35	60	112.6	2015	6.00	9956	97.3	0	3.1	±0.4
NP05.07	674	15	6.87	45	190.0	1244	5.62	11971	95.5	0	3.4	±0.5
NP05.08	739	22	0.30	49	15.6	2884	6.00	9956	65.2	1	1.7	±0.2
NP05.09	1540	21	0.58	12	49.6	1019	6.00	9956	90.2	1	1.2	±0.4
NP05.10	1621	23	1.86	42	71.7	1314	6.00	9956	79.6	2	2.7	±0.4
NP05.11	1582	24	2.69	63	182.3	4265	6.00	9956	40.2	12	1.5	±0.2
NP05.12	1600	25	1.59	39	190.3	4676	6.00	9956	0.3	76	0.9	±0.2
NP05.13	1600	16	0.32	5	21.6	339	6.00	9956	14.9	1	1.5	±0.7
NP05.14	1833	30	0.71	21	209.9	6190	6.00	9956	15.1	49	0.4	±0.1
NP05.15	1180	21	3.92	81	140.0	2890	6.00	9956	80.7	0	2.9	±0.3
NP05.17	770	11	1.36	11	60.1	221	6.62	11971	95.0	0	2.1	±1.0
NP05.18	2027	18	3.17	43	172.5	2343	6.00	9956	99.9	0	1.9	±0.3
NP05.20	1935	9	4.57	37	90.3	731	6.00	9956	90.3	0	4.7	±0.8
NP05.21	2360	17	8.83	138	143.2	2238	6.00	9956	72.3	0	6.5	±0.6
NP05.22	2500	22	19.7	419	287.2	6097	6.00	9956	84.1	0	7.2	±0.4
NP05.23	2190	18	21.9	385	264.6	4655	6.00	9956	47.0	7	8.6	±0.5
NP05.24	1350	22	11.3	78	201.3	1389	6.00	9956	81.4	1	5.9	±0.7
NP05.28	330	90	5.51	362	95.7	6284	5.62	11971	4.5	24	5.4	±0.4
T6	1825	16	1.78	25	125.6	1766	5.93	12513	94.6	0	1.4	±0.3
T7	2000	19	2.22	37	158.8	2641	5.93	12513	96.7	0	1.4	±0.2
T9	1780	16	1.73	17	124.9	1225	5.93	12513	95.4	0	1.4	±0.3
T10	2540	17	2.21	29	131.6	1729	5.93	12513	84.4	0	1.6	±0.3
T11	2960	14	1.02	12	72.0	849	5.93	12513	95.9	0	1.4	±0.4
T13	3640	18	1.74	29	117.4	1955	5.67	12016	97.1	0	1.4	±0.3
T14	4500	21	1.03	19	49.6	916	5.67	12016	92.0	0	1.9	±0.5
T15	4260	18	1.58	26	57.6	945	5.67	12016	67.0	0	2.6	±0.5
T17	3260	16	2.11	33	109.3	1708	5.67	12016	98.5	0	1.8	±0.3
NP05.41	**1550**	**25**	**0.47**	**11**	**151.5**	**3559**	**5.62**	**11971**	**95.0**	**0**	**0.3**	**±0.1**
NP05.42	**1450**	**25**	**0.87**	**20**	**92.9**	**2137**	**5.62**	**11971**	**96.5**	**0**	**0.9**	**±0.2**
NP05.44	**1130**	**27**	**1.19**	**26**	**137.2**	**3002**	**5.62**	**11971**	**94.3**	**0**	**0.8**	**±0.2**
NP05.50	**1140**	**18**	**4.04**	**45**	**158.0**	**1758**	**5.62**	**11971**	**98.0**	**0**	**2.4**	**±0.4**

[a]N, number of individual grains dated; ρ_s, spontaneous track density; N_s, spontaneous track counted; ρ_i, induced track density in external detector (muscovite); N_i, number of induced track counted; ρ_d, induced track density in external detector attached to dosimeter glass; N_d, number of tracks counted in determining ρ_d; P(χ^2), chi-square probability; D, age dispersion. All reported ages are central ages [*Galbraith and Laslett*, 1993] ±1 standard deviation. Note that zero-track grains were abundant and included in the age determinations. Sample preparation followed standard methods [cf. *van der Beek et al.*, 2006]. All ages were determined by XR using a zeta calibration factor of 350 ± 7 for glass standard NBS962. Ages in normal font were previously reported by *Robert et al.* [2009]; those in bold are new. For details on sample location, lithology, etc., see Table S1.

across the MCT zone, as well as local age-elevation profiles sampled orthogonally to the tectonic transport direction in order to limit complications due to nonvertical particle paths [e.g., *Huntington et al.*, 2007]. We targeted quartzites of the Kushma, Kuncha and Nourpul formations (Proterozoic Nawakot Group) [*Upreti*, 1999] as well as the ~1830 Ma [*DeCelles et al.*, 2000] Ulleri gneiss and the Miocene [*DeCelles et al.*, 1998] Dumri formation in the Lesser Himalaya. In the Langtang transect, we exploited the fact that the transect crosses the Higher Himalayan crystalline Kathmandu klippe to sample the Ordovician [*Gehrels et al.*, 2006] Palung granite intruded into it.

[21] Twenty-seven AFT ages from the Langtang-Hetauda transect, including two age-elevation profiles at Mount Gosainkund in the MCT zone (Langtang Himal) and through the Palung granite, were reported by *Robert et al.* [2009]. We sampled and processed sixteen additional samples along the Annapurna-Buthwal transect, including an age-elevation profile at Ghorepani Hill (Lesser Himalaya in the topographic transition zone just south of the Annapurna massif). However, twelve of these samples, mostly from the Lesser Himalaya, could not be dated. The majority of undatable samples are white quartzites from the Nawakot Group, which either do not contain sufficient apatite, or apatite that is so poor in Uranium that no spontaneous or

induced fission tracks were recorded. For completeness, all dated samples are reported in Table 1; information on all collected samples is provided in the auxiliary material (Table S1).[1]

[22] We complete our database for the Annapurna-Buthwal transect with extensive AFT data from the Marsyandi valley ~50 km to the east [*Burbank et al.*, 2003; *Blythe et al.*, 2007]. This database contains 82 AFT ages and several age-elevation profiles, which were, however, exclusively sampled in Higher Himalayan crystalline rocks. For the Langtang-Hetauda transect, we complete our AFT data with mica Ar-Ar data from *Arita et al.* [1997], *Rai* [1998], and *Bollinger et al.* [2004] (cf. compilation by *Herman et al.* [2010]) as well as 10 AFT ages recently reported by *Herman et al.* [2010]. Finally, we include an extensive AFT data set from Bhutan [*Grujic et al.*, 2006] comprising 45 AFT ages, again all from the Higher Himalayan crystalline series, in our analysis. The different north-south transects through the Himalayan range are compared by projecting each transect on a profile normal to the MFT (Figure 3).
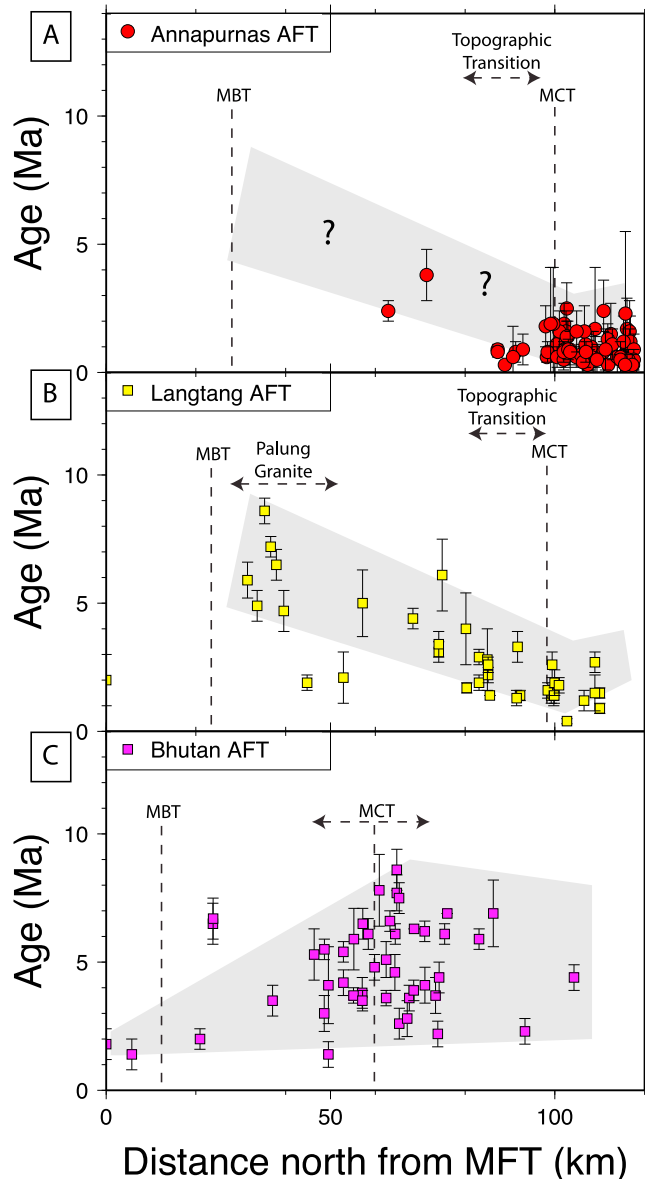
Figure 3. AFT data sets projected onto profiles perpendicular to the MFT. Locations of samples are indicated in Figure 2. Error bars show 1σ errors. (a) Annapurna-Buthwal transect; data principally from *Blythe et al.* [2007] augmented by four new AFT ages from the Kali Gandaki valley and the Lesser Himalaya (Table 1). (b) Langtang-Hetauda transect; data from *Robert et al.* [2009] (reported in Table 1 for completeness) augmented by 10 ages obtained by P. Copeland and reported by *Herman et al.* [2010]. (c) Bhutan Himalaya; data from *Grujic et al.* [2006]. The gray areas in Figures 3b and 3c outline the trends of AFT ages for the Langtang-Hetauda and Bhutan transects, respectively. To compare the Langtang-Hetauda and the Annapura-Buthwal sections, we also plot the trend for the Langtang-Hetauda transect (Figure 3b) in Figure 3a (Annapurna Buthwal transect), where question marks indicate zones without data.

3.2. AFT Age Patterns

[23] The most continuous age trend has been obtained for the Langtang-Hetauda transect. AFT ages plotted as a function of distance to the MFT show a continuous trend, in which ages young nearly linearly from the MBT to the MCT (Figure 3). The northernmost samples, from the MCT zone in Langtang, are very young (<3 Ma), indicating strong local exhumation. This trend crosses the topographic transition and the MCT zone without a significant jump in ages. *Robert et al.* [2009] discussed the interpretation of the data from this transect, including two age-elevation profiles, in detail. An age-elevation profile from the Palung granite (Kathmandu klippe in the Lesser Himalaya) shows an exhumation rate of 0.5 ± 0.1 km My^{-1}. In contrast, an age-elevation profile from the MCT zone (Gosainkund Mountain) suggests an apparent exhumation rate an order of magnitude higher, at $4.4^{+4.8}_{-1.5}$ km My^{-1}, comparable with strike-parallel age-elevation relationships observed in the Marsyandi area [*Blythe et al.*, 2007]. However, at such high rates of exhumation, topographic disturbance of the closure isotherm may lead to severe overestimates of exhumation rates from age-elevation relationships [*Stüwe et al.*, 1994; *Mancktelow and Grasemann*, 1997; *Braun*, 2002; *Ehlers*, 2005]; we estimate real exhumation rates for the Gosainkund profile to be on the order of 2.0–2.5 km My^{-1} [*Robert et al.*, 2009]. These exhumation rates are consistent with overthrusting at a rate of 5–6 km My^{-1} over a ~20° dipping crustal ramp in the MCT zone and a ~5° dipping flat for the Palung granite. *Herman et al.* [2010] recently reached a similar conclusion, based on modeling the existing thermobarometric, Ar-Ar, and AFT data along the same transect. Thus, the data from the Langtang transect do not appear to require active out-of-sequence thrusting in the MCT zone or the topographic transition and are compatible with the ramp flat geometry of the MHT as constrained by independent geophysical and geodetic data as described in section 2.1. We will assess this assertion using numerical modeling in section 4.2.

[24] The age pattern for the Annapurna-Buthwal transect is less well constrained than that for the Langtang transect because of a lack of data in the Lesser Himalaya, in spite of our efforts to sample this region. *Hodges et al.* [2004] suggested that an observed jump in AFT ages across the MCT zone requires out-of-sequence reactivation at this latitude. However, a comparison of AFT ages projected along a line perpendicular to the MFT shows a similar trend for both transects (Figure 3): ages from the MCT zone are similar (but slightly younger in the Annapurnas compared to Langtang). In the Lesser Himalaya, only two AFT ages were obtained south of the topographic transition, but these are similar to ages from similar structural positions in the Langtang-Hetauda transect. The rate of increase in ages toward the south in the Lesser Himalaya is also similar in both transects (0.1 to 0.2 My km^{-1}). They thus appear, to a first order, compatible with a similar geometry and kinematics of the MHT as for the Langtang transect.

[25] A projection of *Grujic et al.*'s [2006] AFT data from Bhutan does not show a very regular trend, even if we use separate projections for the data from western and eastern Bhutan. As noted by *Grujic et al.* [2006], AFT ages are generally older than in central Nepal. Moreover, the pattern appears to be opposite to that observed for Nepal (Figure 3):
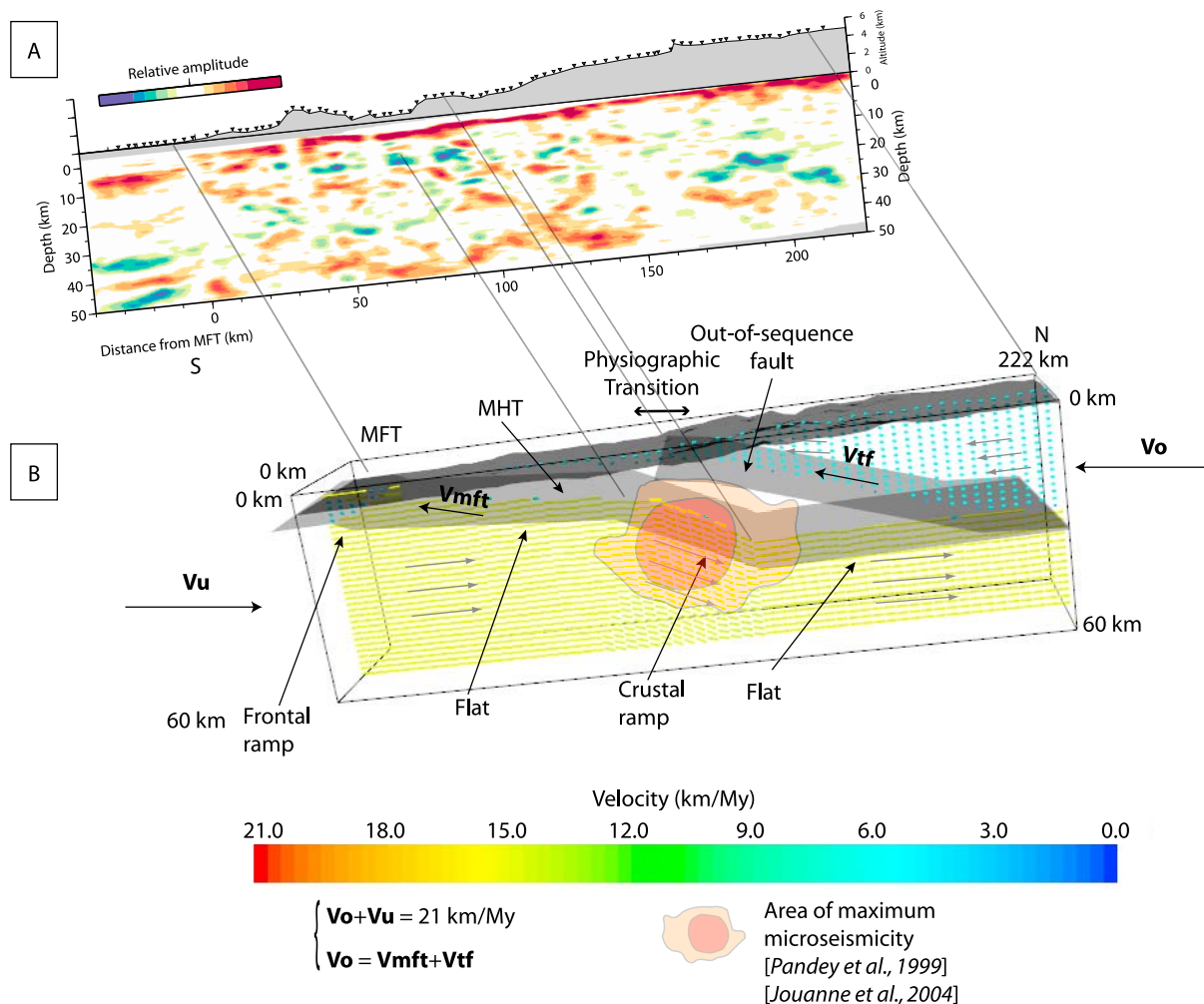
Figure 4. (a) Receiver function image showing the principal contrasts within the lithosphere [*Nabelek et al.*, 2009]. Red and blue colors represent interfaces with increasing and decreasing impedance with depth, respectively. Horizontal distances are referenced to the surface trace of the MFT. All depths are relative to sea level. (b) Initial model geometry proposed from geophysical data with major structure and kinematic partitioning shown by colored arrows. The crustal ramp is inferred from the microseismic data of *Pandey et al.* [1999]. Vu and Vo are the underthrusting velocity and the total overthrusting velocity, respectively; the latter is partitioned between the MFT velocity (Vmft) and the out-of-sequence velocity (Vtf). For this initial model show, Vtf = 6 km My^{-1} (light blue arrows), Vmft = 0, and Vu = 15 km My^{-1} (yellow arrows).

AFT ages increase from south to north in Bhutan, whereas they decrease in Nepal. This first-order observation suggests that rocks exposed at the orogenic front in Bhutan are exhumed more rapidly than those in the region of highest topography. No AFT age inflexion is observed in this profile. The AFT age pattern observed in Bhutan appears to imply that (1) there is no reactivation of the MCT, (2) the MHT does not comprise a crustal ramp below the region of highest topography, and (3) the overall dip of the MHT is lower than in Nepal. The Bhutan Himalaya has served as the type area where geological evidence for the "channel flow" model has been collected [*Grujic et al.*, 2002]. Currently active channel flow in the Bhutan Himalaya should be marked by very young AFT ages in the MCT zone and in the Higher Himalaya and appears excluded by the data. The

data do, however, allow channel flow operating before 12–10 Ma, as proposed by *Hollister and Grujic* [2006].

4. Thermokinematic Model

4.1. Forward Model Description

[26] In order to assess the above qualitative interpretations of the AFT age patterns more quantitatively, we develop both forward and inverse numerical models. We employ a modified version of *Pecube* [*Braun*, 2003], a finite element code that predicts thermochronological ages by solving the three-dimensional (3-D) heat transport equation in a crustal block affected by vertical and/or horizontal advection and characterized by evolving surface topography. New features in the code include the incorporation of faults and associated kinematics (Figure 4). Faults define different crustal blocks

and act as barriers to advection: no matter is advected through the fault surfaces. Faults are defined in the model by their surface trace and a number of points that define their (laterally constant) profile. The velocity field is calculated using a kink band model originally developed by *Braun et al.* [1994] and honors the conservation of mass (see auxiliary material for more details). As in other thermokinematic models for the Himalaya [*Bollinger et al.*, 2006; *Brewer and Burbank*, 2006; *Wobus et al.*, 2006; *Whipp et al.*, 2007] (compare Robert et al., submitted manuscript, 2011, for a review), we use a reference frame fixed to the MHT. If other faults are present, we must take in account the advection of the position (and potentially the geometry) of one fault with respect to the other: the faults are advected and deformed along with the block they occur in due to motion on the MHT.

[27] In order to capture topographic effects on thermochronological age variability, we couple the essentially 2D kinematic model to a planform surface topography, derived from SRTM 90 m digital elevation models of the zones of interest (downgraded to the model resolution of 1 km). Models are run for 10 My, as we concentrate on predicting the AFT age pattern and all AFT ages are <10 Ma. We start from a steady state thermal structure for the kinematics defined at 10 Ma and then predict the transient thermal structure through the model run. Particle paths are tracked through time for rocks that end up at the surface at the end of the model run; the resultant time-temperature paths are used to predict AFT ages using the fission track annealing model of *Green et al.* [1989] with the modified annealing parameters of *Stephenson et al.* [2006].

[28] We assume the topography to be in steady state in the models presented here. In consequence, we are not able to test the role of changes in relief through time. There are two main reasons for this approach. First, *Valla et al.* [2010] have shown that AFT data alone are not very sensitive to relief changes; even in fairly simple tectonic and topographic settings they must be combined with lower-temperature thermochronometers to constrain these. Second, *Galy et al.* [2010] have recently shown, using multiple isotopic data from the Bengal Fan, that the erosion patterns, drainage systems and mean elevation of the Himalaya and southern Tibetan plateau have remained relatively stable for the last 12 My, despite major climatic changes during this time span.

[29] The initial model geometry is based on the inferred structure of the MHT in central Nepal [*Cattin and Avouac*, 2000; *Avouac*, 2003; *Pearson and DeCelles*, 2005], i.e., a flat ramp flat geometry with the midcrustal ramp located below the topographic transition between the Lesser and the High Himalaya (Figure 4). The crustal ramp is situated by the slope break in the interpreted receiver function cross section of central Nepal [*Nabelek et al.*, 2009] (Figure 4b) and the area of maximum microseismicity (Figure 4a and *Pandey et al.* [1999]). The MHT is active throughout the model run. Due to the proximity of the MBT and the MFT, we consider these as a single fault in order to simplify the models. Previous thermokinematic models for the central Nepal Himalaya have shown that, for a reference frame fixed to the MHT, observed thermochronological ages require overthrusting velocities of 5–6 km My^{-1} [*Bollinger et al.*, 2006; *Brewer and Burbank*, 2006; *Whipp et al.*, 2007]

(compare Robert et al., submitted manuscript, 2011, for a review), implying underthrusting of the Indian plate at a velocity of ~15 km My^{-1} in order to obtain a total convergence rate of 20–21 km My^{-1} [e.g., *DeCelles et al.*, 2001; *Mugnier et al.*, 2004; *Mugnier and Huyghe*, 2006]. Here we will use overthrusting and underthrusting velocities of 6 and 15 km My^{-1}, respectively, although we present model runs with different partitioning in order to study its effect on predicted age patterns. The geometry of the MHT is allowed to vary between different models (see below) and, for the central Nepal models, we include a separate fault that breaks to the surface at the front of the topographic transition in order to simulate out-of-sequence thrusting (Figure 4).

[30] Note that, because no material is allowed to cross the MHT in our models, and both the MHT and the topography are fixed, we do not include underplating of Indian plate material as modeled by *Bollinger et al.* [2006] and *Herman et al.* [2010]. *Bollinger et al.* [2006] propose an underplating model with the development of a duplex at midcrustal depth to explain the well-known inverse metamorphic gradient below the MCT. The main difference between models including underplating and simple overthrusting models is that the former allow steepening of particle paths (and therefore younging of thermochronological ages) above the underplating window without requiring a ramp in the crustal-scale detachment. However, inclusion of underplating mainly affects higher-temperature thermochronometers such as mica ^{40}Ar/^{39}Ar; low-temperature thermochronometers such as AFT, for which the closure depth lies well above the crustal ramp (or underplating window) record fairly similar kinematics for both models. Therefore, a simple overthrusting model as developed here explains low-temperature (AFT) thermochronology data just as well as the more elaborate models [*Brewer and Burbank*, 2006; *Whipp et al.*, 2007].

4.2. Forward Model Results

[31] Figure 5 shows forward model geometries and predicted AFT ages for a simple overthrusting model, as well as models including out-of-sequence thrusting at different velocities, applied to the Langtang transect. In these models, overthrusting takes place along the MHT for the first 8 My of the model run and is subsequently partitioned between the MHT and the out-of-sequence thrust for the last 2 My, in order to simulate Quaternary reactivation of the MCT zone (as suggested by *Hodges et al.* [2004]). As expected, AFT ages in the Lesser Himalaya become older with increasing activity of the out-of-sequence thrust and consequent decrease of velocity on the MHT; for $V_{TF} \geq 4$ km My^{-1}, AFT ages in the southern part of the Lesser Himalaya are unreset since 10 Ma. However, except for these extreme models, where nearly all overthrusting is taken up on the out-of-sequence thrust, the models do not predict a clear age jump at the topographic transition zone. This is because out-of-sequence thrusting has not been going on for long enough in these models to influence the AFT ages in the Lesser Himalaya, which are mostly around 5 Ma. Surprisingly, models including the most rapid overthrusting also predict older ages within the hanging wall of the out-of-sequence thrust. This is because the hanging wall of the out-of-sequence thrust is much thinner in the MCT zone than the hanging wall of the MHT, so that the thermal perturbation associated with overthrusting is much smaller, and the near-
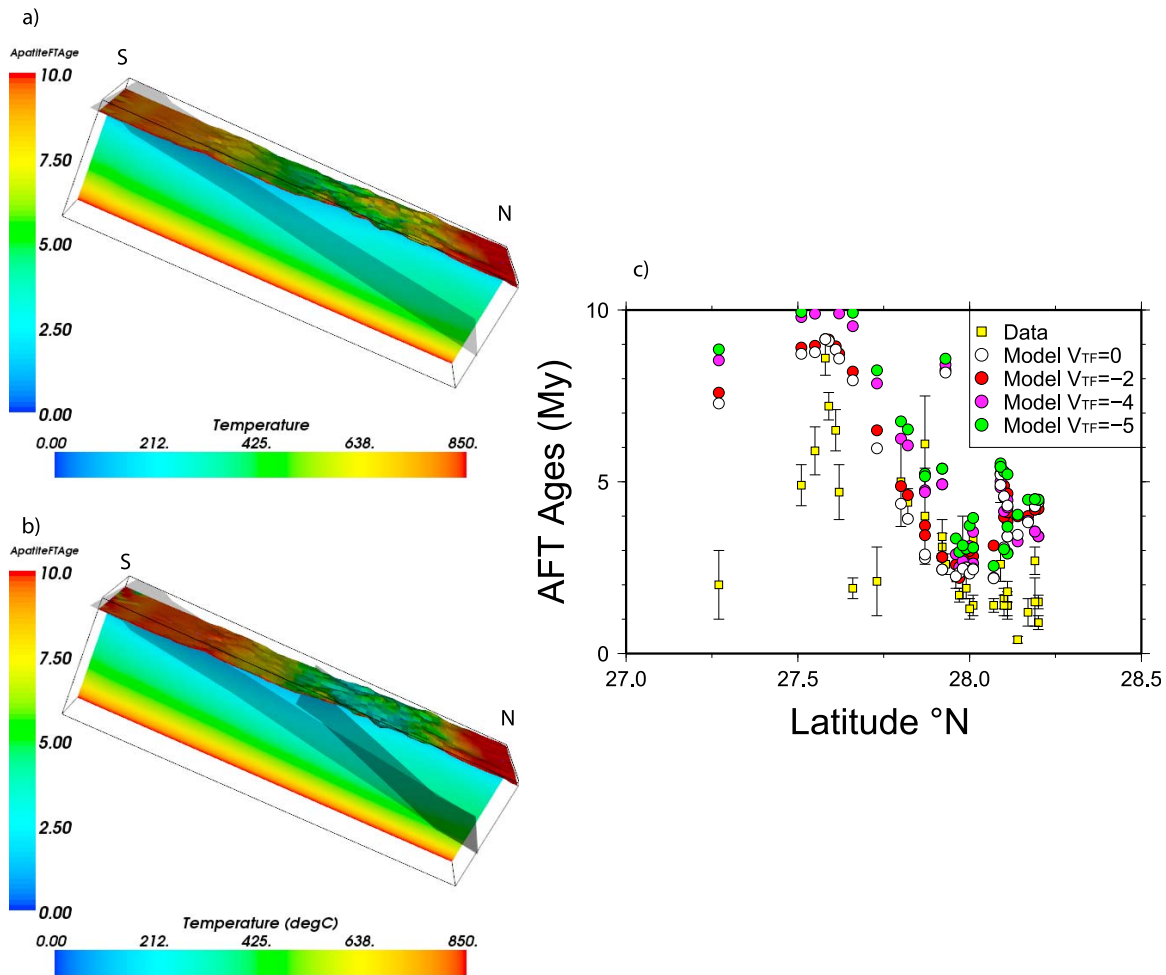
Figure 5. (a) Forward model geometry for the Langtang transect showing the modeled MHT, model kinematics and predicted thermal structure and AFT age pattern at the surface for a model of overthrusting on the MHT ($V_0 = 6$ km My^{-1}). (b) Same as Figure 5a but for a model including out-of-sequence thrusting on a fault breaking the surface at the front of the topographic transition ($V_{TF} = 5$ km My^{-1}). (c) Comparison of observed and predicted AFT age patterns for the Langtang transect as a function of out-of-sequence thrusting velocity (V_{TF}); the overthrusting velocity on the MHT is equal to $(6 - V_{TF})$ km My^{-1} in these models.

surface thermal gradient consequently lower, when a significant part of the overthrusting velocity is taken up by the out-of-sequence thrust (compare Figures 5a and 5b). None of these forward models fit the observed AFT age pattern particularly well, however, probably because the model geometry and thermal parameters can be improved.

4.3. Inverse Models

[32] The thermochronologic age predictions depend on the fault geometry and kinematics as well as the thermal structure of the modeled crustal block. In order to explore this complex multidimensional parameter space, we couple *Pecube* with the Neighborhood Algorithm (NA) inversion routine [*Sambridge*, 1999a, 1999b], using the approach developed by *Braun and Robert* [2005] and *Valla et al.* [2010]. The NA inversion scheme can be used both to seek an optimum set of parameters to explain the data and to evaluate the sensitivity of model predictions to the values of the input parameters. NA performs an intelligent search to

find the set of parameter values of a given model that will minimize the difference between model predictions and measured ages.

[33] In the following, we will present seven sets of inversions that aim to constrain the geometry of the crustal detachment, the kinematics of deformation and the thermal structure of the crust. In an initial inversion, we allowed the basal temperature (T_0) and normalized heat production (Q) to vary; however, this led the model to converge on a geologically unrealistic set of parameters (see below). Subsequent inversions therefore fix the thermal parameters to reasonable values. The MHT geometry is modified by allowing variations in the x and y positions (i.e., the distance from the MFT and the depth) of both the top and the base of the midcrustal ramp within the bounds set by the geophysical data [*Pandey et al.*, 1999; *Nabelek et al.*, 2009] (Figure 4). Finally, in models including an out-of-sequence thrust, we allow partitioning of the overthrusting velocity
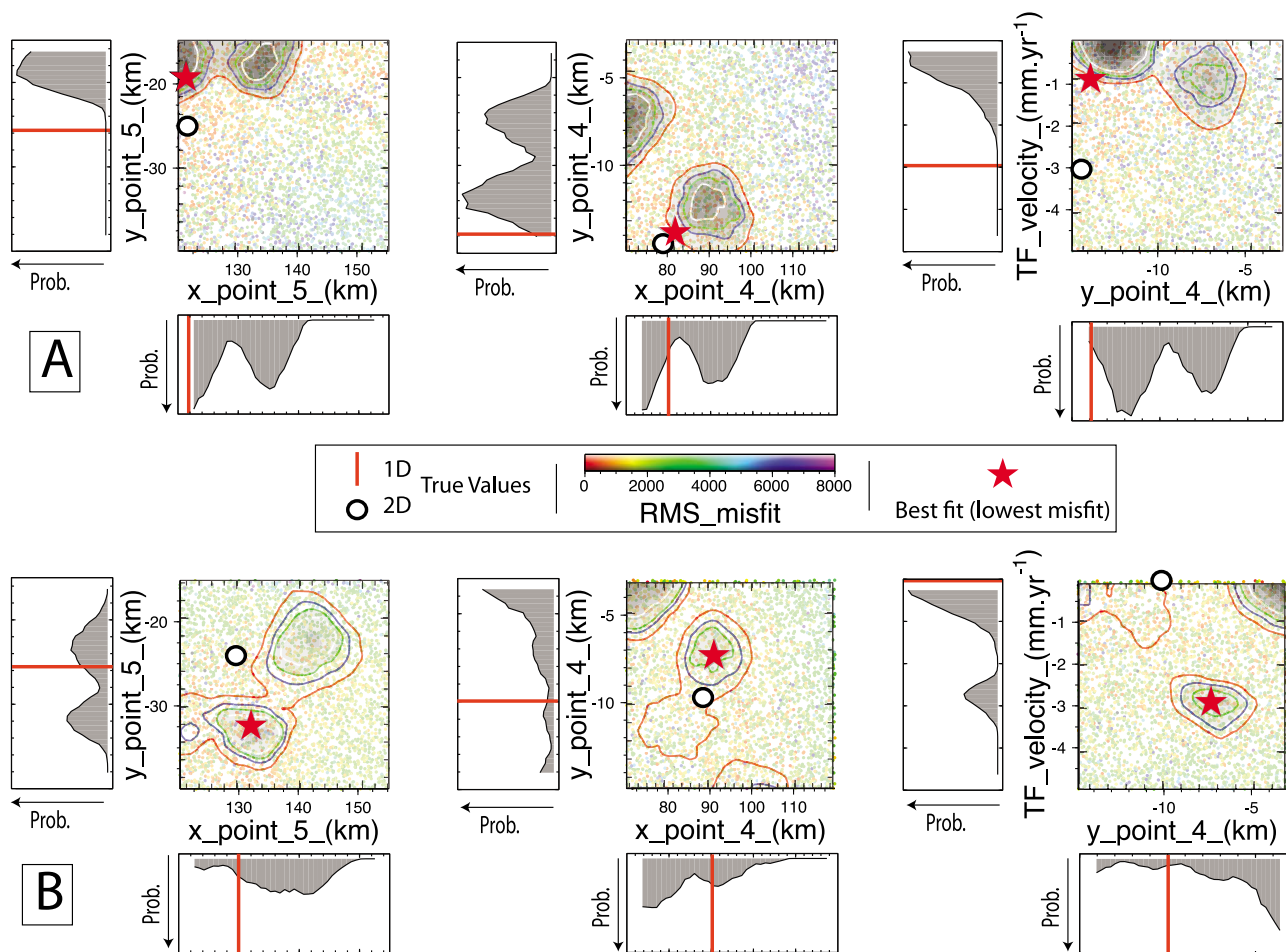
Figure 6. (a and b) Scatter diagrams showing results of NA inversions using a Monte Carlo method for two sets of synthetic inversions using the results from two synthetic models as input (each inversion was performed with 2550 forward model runs). One-dimensional posterior pdfs obtained by the NA appraisal stage are shown adjacent to the axes for each parameter. Two-dimensional posterior pdfs also obtained by the NA appraisal stage are shown with contour lines overlying the scatter diagrams, where the gray scale corresponds to the probability density, and the red, blue, green, and black contours correspond to the 95%, 75%, 60%, and 40% confidence intervals, respectively. The input parameter values are shown on the 1-D pdfs with a red line and on the scatterplots/2-D pdfs with a white circle. The red star corresponds to the lowest misfit found.

(V_o) between motion on the out-of-sequence thrust (V_{TF}) and the MHT ($V_o - V_{TF}$) (Figures 4 and 5).

[34] We use a misfit function that is defined by the L_2 norm of the weighted difference between the observation vector, O, and the prediction vector, P:

$$misfit = \sum_{i}^{n} \left(\frac{O_i - P_i}{\Delta O_i} \right)^2$$

where ΔO_i are the observational errors, taken here as the 1σ errors on the AFT ages. This search necessitates a large number of model runs to sample a large combination of parameter values. Using a high-performance cluster, we were able to perform several thousand forward model runs in a reasonable amount of time. In order to extract the sensitivity of the model to the different parameters, we use the NA-Bayes approach [*Sambridge*, 1999b], which pro-

duces probability density functions (pdf) for each parameter over the entire parameter space, by using Bayesian integrals and the misfit results.

[35] In order to test the ability of the inversion method to recover the input model values, we performed two sets of synthetic inversions using as input the AFT results of two end-member synthetic models, one in which overthrusting takes place solely on the MHT, including a 20° dipping midcrustal ramp; the other in which 50% of the over-thrusting velocity is taken up by out-of-sequence motion on the MCT (Figures 6 and 7). Forward models predict AFT ages at the locations of our data for the Langtang transect; we subsequently invert these synthetic data in order to assess the capacity of the approach to retrieve the "true" input parameters. Results from these synthetic inversions do not converge to unique solutions for most parameters, and the lowest misfit (the "best" model) does not necessarily correspond to the mode of the parameter pdf (the "most
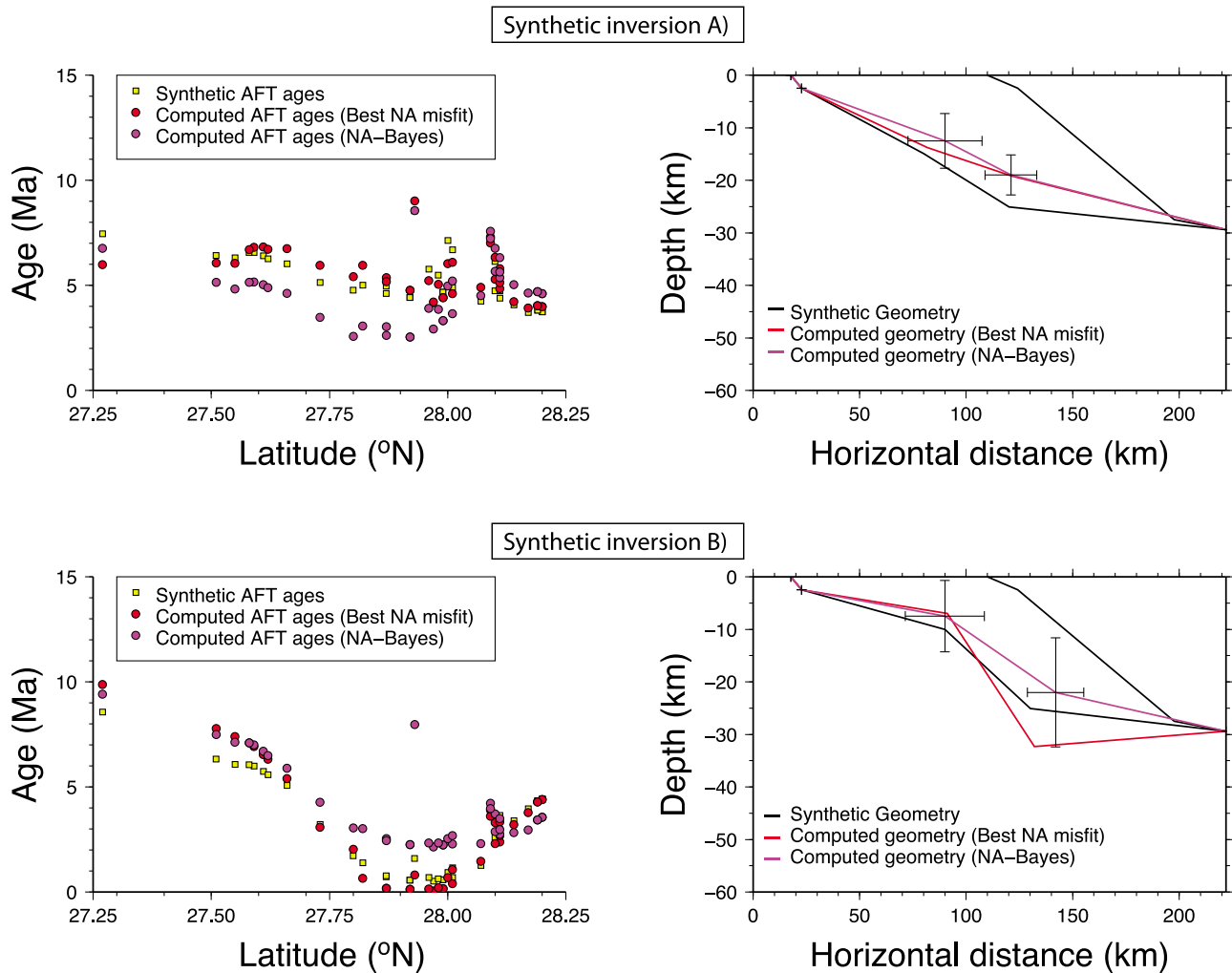
Figure 7. (a and b) Comparison for the synthetic inversions (Figure 6) of the synthetic AFT ages and geometry to the predicted AFT ages and geometry with the best models (best NA misfit is model with the lowest misfit; NA-Bayes is mode of parameter pdf's from NA-Bayes output). Black crosses show the 2σ error on the most probable parameter values given by NA-Bayes.

probable" model). However, in both synthetic inversions, the geometrical parameters are relatively well reproduced with <5 to 28% difference between input parameter values and retrieved best fit values. The out-of-sequence velocity parameter is not so well constrained: for the model including out-of-sequence thrusting, neither the "most probable" nor the "best" models reproduce the true input value (70 to 95% difference; Figure 6a), whereas for the model without out-of-sequence thrusting, the pdf fits well with the true value (1% difference; Figure 6b). We conclude that our inversions constrain geometrical parameters relatively well, but that the kinematic predictions (in particular the presence or absence of a component of out-of-sequence thrusting) are less reliable.

4.4. Inverse Model Results

4.4.1. Geometry of the MHT and Importance of Out-of-Sequence Thrusting

[36] In order to search for the best fitting combination of thermal, geometric and kinematic parameters, we ran an initial inversion in which we allowed the basal temperature

to vary between 500 and 1500°C and the "normalized heat production" between 1 and 5 (corresponding to minimum and maximum depth-averaged heat production rates of 0.25 and 3.80 μW m^{-3}, respectively). The "normalized heat production" is a nondimensional parameter that scales the crustal heat production to the model thickness, the thermal diffusivity and the basal temperature [cf. *Batt and Braun*, 1997]. We search for the optimum partitioning between frontal and out-of-sequence thrusting by letting V_{TF} vary between 0 and 5 km My^{-1} and we allow the MHT geometry to vary between the limits imposed by the geophysical data, as described above. We ran 100 generations of 100 models each for this inversion, giving a total of 10,100 models (including an initial "seed" of 100 models). The model is fit to the set of AFT ages shown in Figure 5, as well as 45 mica Ar-Ar ages reported by *Arita et al.* [1997], *Rai* [1998], and *Bollinger et al.* [2004]. However, since the spatial distribution of the latter is not optimal, they do not constrain the models much more than the AFT data alone.

[37] The results of this initial inversion are presented in Figure 8 and the parameter combination for the best fit
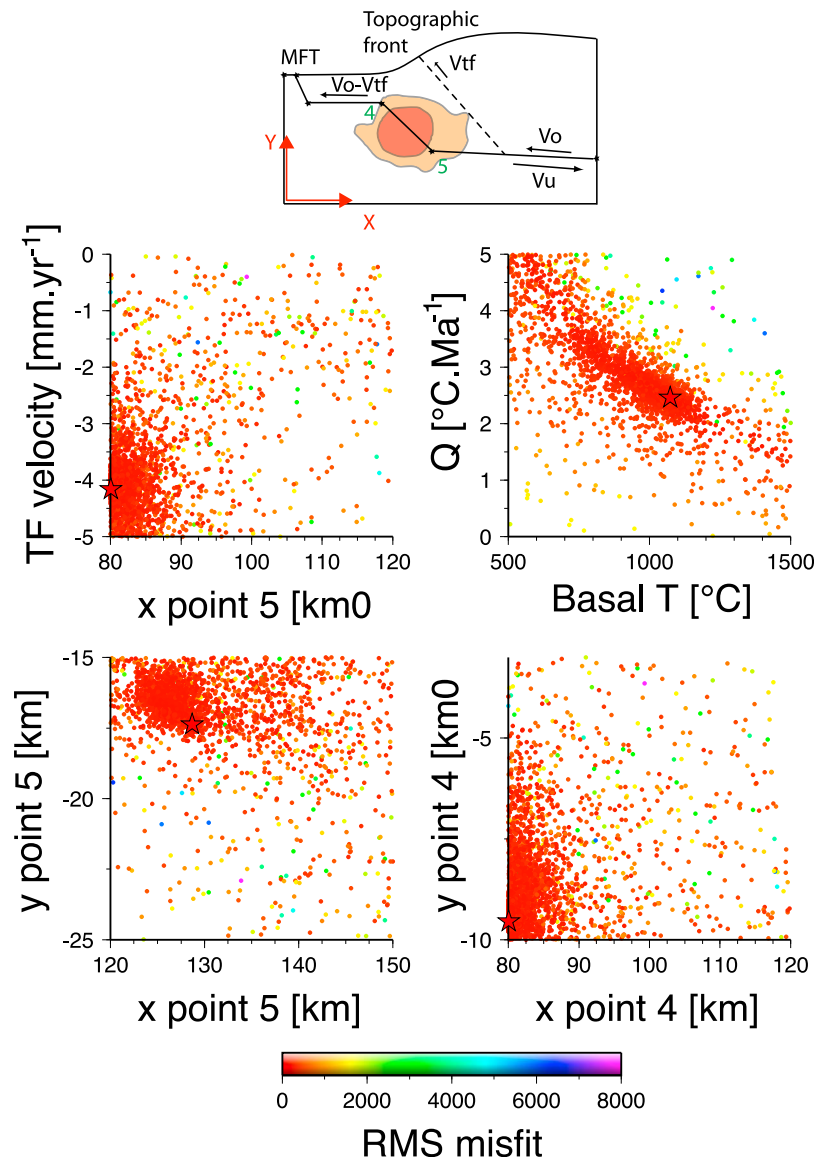
Figure 8. Initial inversion results for the Langtang transect. Results are shown as two-dimensional sections through the parameter space, in which each model (parameter combination) is represented by a dot colored according to the misfit between predicted and observed data. Star shows location of best fit model reported in Table 2; TF velocity is the velocity of the out-of-sequence thrust, Q is the normalized heat production, basal T is the basal temperature, and x point i/y point i is the position of the points i which define the geometry of the MHT (see upper sketch for definition of these points).

model is reported in Table 2 (model LT1). This initial inversion leads to optimal solutions in which a significant amount of overthrusting is taken up by the out-of-sequence thrust since 2 Ma (V_{TF} = 4.2 km My^{-1} for the best fit model) with a weakly expressed midcrustal ramp (ramp dip of 9° versus a shallow detachment dip of 6°). However, optimal solutions also lead to an unrealistically "hot" crust, with a best fit basal temperature of 1100°C at 65 km depth and a stable (in the absence of heat advection) near-surface geothermal gradient of 63°C km^{-1}. Although there is a clear tradeoff between basal temperature and heat production in these models, all optimal solutions are characterized by unrealistically high surface geothermal gradients.

[38] We therefore proceeded to run a set of less general inversions, in which we fixed the thermal parameters at T_0 = 850°C and Q = 1.5 (corresponding to a depth-averaged heat production rate of 0.65 μW m^{-3}), in order to predict a reasonable stable near-surface geothermal gradient of 35°C km^{-1}. We ran a smaller number of models for these inversions (i.e., 50 initial models and then 50 generations of 50 models each, for a total of 2550 models) because they appear to converge to an optimal solution relatively rapidly. The geometric and kinematic parameters were allowed to vary as before. The results for this inversion (LT2; reported in Table 2) are opposite to the initial ones in that optimal models have practically no out-of-sequence thrusting (V_{TF} =

Table 2. Inversion Parameters and Results

	Inversion						
	LT1	LT2	LT3	LT4	AN1	AN2	BU1
Area	Langtang	Langtang	Langtang	Langtang	Annapurnas	Annapurnas	Bhutan
No of models	10100	2550	2550	2550	2050	410	328
Best misfit	320	157	157	157	54	40	1620
T_0 (°C)	**1100**	850	850	850	850	**1300**	**714**
Q	**2.5**	1.5	1.5	1.5	1.5	**2.6**	**3.9**
Grad(T) (°C km^{-1})	**63**	35	35	35	35	**70**	**52**
V_0 (km My^{-1})	−6	−6	−8	−8	−6	−6	−6
O.o.S. timing (Ma)	2 - 0	2 - 0	2 - 0	4 - 0	2 - 0	-	-
V_{TF} (km My^{-1})	-4.2	-0.2 (−0.8 ± 0.8)	-7.8	0	0 (−3.1 ± 1.9)	-	-
$X4$ (km)	80	80 (101 ± 14)	85	80	110 (94 ± 11)	97	117
$Y4$ (km)	-9	-3 (−8 ± 5)	-14	-3.5	-6 (−8 ± 2)	-5	-7
$X5$ (km)	129	150 (133 ± 6)	150	150	150 (135 ± 11)	140	147
$Y5$ (km)	-17	-28 (−26 ± 4)	-27	-27	-30 (−16 ± 4)	-23	-17
Flat dip (deg)	**6.2**	6.2 (4 ± 9.2)	11.0	1.0	0.3 (7 ± 8)	2.0	5
Ramp dip (deg)	**9**	20 (30 ± 18)	11	19	34 (11 ± 4.6)	21	7

Numbers in bold represent the values of the free parameters for the best fit model, other parameters are kept constant. Values of free parameters with 1σ errors in parentheses correspond to the results given by NA-Bayes; single values correspond to the lowest misfit found. The stable near-surface geothermal gradient (grad(T)) in the absence of heat advection, and the dips of the MHT ramp and southern (shallow) flat have been computed for each model in order to compare parameter values to observables. O.o.S. timing is timing of onset of out-of-sequence thrusting; X i/Y i are position of the points i that define the geometry of the MHT ramp and southern flat.

0.2 km My^{-1} for the best fit model). Optimal models issued from the NA inversion fit the data better than those of the first inversion (minimum misfit value of 157 versus 320). The geometry of the MHT (shallow flat dip of 6° and ramp dip of 20°) is in good agreement with what is known from geophysical and geodetic data [e.g., *Schulte-Pelkum et al.*, 2005; *Nabelek et al.*, 2009]. For model LT2, we have run the NA appraisal code with a Monte Carlo inversion to extract the posterior pdf for each parameter (Figure 9a). Table 2 shows that the modes of the 1D and 2D pdfs for the geometrical parameters are close to the NA inversion results (<11% difference except for the depth of point 4, for which the difference is 80%) and that the range of the acceptable value for those parameters is relatively well defined (less than 15% range). However, the result for the out-of-sequence velocity is less constrained: it only shows that V_{TF} is lower than 1.6 km My^{-1} (with 95% confidence).

[39] In a third inversion (LT3), we explore the influence of changing the partitioning between overthrusting and underthrusting on the MHT by running an inversion where the total overthrusting velocity is fixed at 8 km My^{-1} (with a corresponding underthrusting velocity of 13 km My^{-1}). All other parameters (both fixed and free) are similar to the previous models. Somewhat surprisingly, this model again favors solutions with significant to near total out-of-sequence thrusting (V_{TF} = 7.8 km My^{-1} for the best fit model) and a purely linear MHT, with both flat and ramp dips of 11° (Table 2). This result is consistent with that obtained by *Herman et al.* [2010], who showed that out-of-sequence models require a higher overall overthrusting velocity to fit the data than models including a crustal ramp. A possible explanation for this puzzling behavior is that the higher overthrusting (and thus exhumation) rates need to be offset by a smaller thermal perturbation in the MCT zone, as predicted by the out-of-sequence model (see above). Another possibility is that the AFT data simply lack the resolution to record reactivation of the MCT zone in the last 2 My.

[40] A final inversion run (LT4) was designed to test the latter assertion, as well as the possible effect of the timing of onset of out-of-sequence thrusting. This timing is not very well constrained by the proponents of recent reactivation in the MCT zone. For instance, although *Hodges et al.* [2004] speak of "Quaternary" faulting, they also relate it to possible increased precipitation and denudation since mid-Pliocene (i.e., 3–4 Ma) times. We thus ran a final inversion in which the onset of possible out-of-sequence thrusting is pushed back to 4 Ma, while maintaining a total overthrusting velocity of 8 km My^{-1}. This final inversion leads again to completely opposite results, namely a total absence of out-of-sequence thrusting (V_{TF} = 0 for the best fit model) and a ramp dip of 19°, very close to that inferred from inversion LT2 (Table 2). The predicted dip of the shallow detachment is very low (1°) in this model, in contrast, in order to accommodate the relatively low exhumation rates recorded by the AFT data in the Lesser Himalaya with the higher overthrusting velocity.

[41] We conclude from the above inversion results that the AFT data in the Langtang transect lack the resolution to formally rule out recent (i.e., Quaternary) reactivation of an out-of-sequence thrust below the topographic transition zone, but seem to exclude an earlier onset of out-of-sequence thrusting. Moreover, such a model requires either unrealistically high crustal temperatures or high total over-thrusting velocities. Finally, significant out-of-sequence thrusting is incompatible with the presence of a midcrustal ramp in the MHT, although such a ramp is inferred from a wealth of structural, geophysical and geodetic data (cf. section 2.1.). In contrast, the data do constrain the geometry of the MHT very well, and best fit models without significant out-of-sequence thrusting (in particular the results of inversion LT2) predict a flat ramp geometry that is in good quantitative agreement with available geophysical and geodetic data. In the next set of model runs, we will thus use this model as a template and study what lateral variations in MHT geometry are required by the data from the transects to the west and east of the Langtang transect.
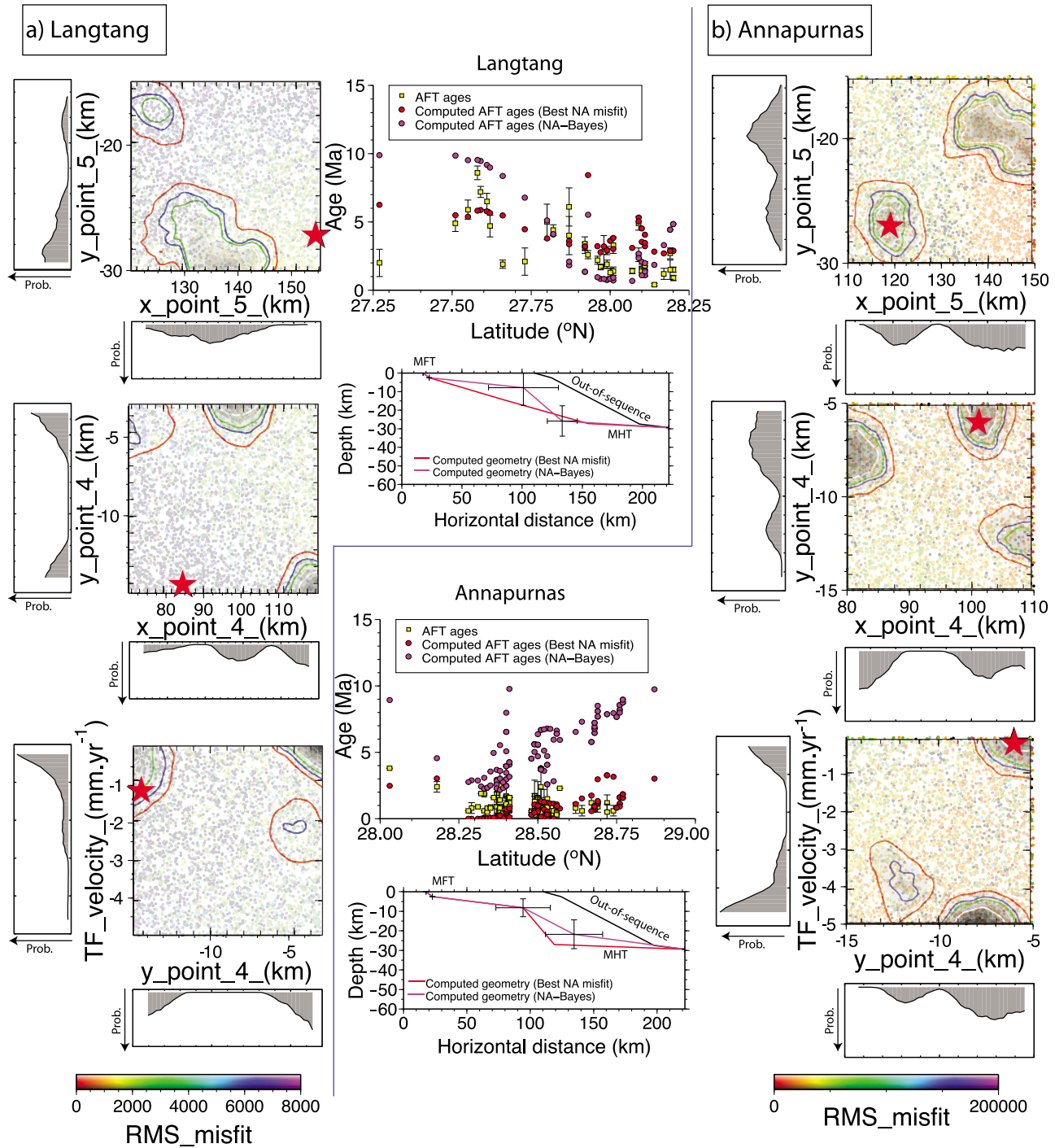
Figure 9. Scatter diagrams showing results of NA inversions using a Monte Carlo method for inversions of (a) Langtang LT2 and (b) Annapurnas AN1 models (2550 forward model runs in each inversion). One-dimensional posterior pdfs obtained by the NA appraisal stage are shown adjacent to the axes for each parameter. Two-dimensional posterior pdfs also obtained by the NA appraisal stage are shown with contour lines overlying the scatter diagrams, where the gray scale correspond to the probability density and the red, blue, green, and black contours correspond to the 95%, 75%, 60%, and 40% confidence intervals, respectively. The red star corresponds to the lowest misfit found. In the middle, AFT ages are also compared to predicted AFT ages for the best fit models and fault geometry is shown for both methods (best NA misfit is model with the lowest misfit; NA-Bayes is mode of parameter values from NA-Bayes output). Black crosses show the 2σ error on the most probable value of the parameters given by NA-Bayes.

4.4.2. Lateral Variations in MHT Geometry

[42] We ran two model inversions for the Annapurna-Buthwal transect (west central Nepal). Inversion AN1 searches exactly the same parameter space as LT2 and leads to similar best fit kinematics without out-of-sequence thrusting ($V_{TF} = 0$ for the best fit model; Figure 9b for Monte Carlo inversions with NA appraisal stage; Table 2), although interestingly a second minimum appears for high out-of-sequence thrusting velocities of ~5 km My^{-1}. The predicted MHT ramp dip is higher, however (34° instead of 20°), as required by the ages reported by *Blythe et al.* [2007] from the Marsyandi valley, which are somewhat younger (with a majority of AFT ages < 1 Ma) than our data from Langtang. Posterior pdfs indicate that the MHT geometry is less well constrained for the Annapurna transect than for the Langtang transect, probably because of the scarcity of data in the Lesser Himalaya for this transect. Several values of geometrical parameters can match the data as shown by bimodal parameter pdfs (Figure 9b), but all predict a ramp dip between 20° and 35°. Since the ramp and flat dips are coupled through the location of the top of the ramp (point 4 defining the geometry of the MHT), this also implies a very low dip (<1°) of the southern detachment.

[43] In a second inversion (AN2), we simplified the kinematics by removing the potential out-of-sequence thrust, but again allowed the thermal structure to vary within the same bounds as for model LT1, in order to test whether the young ages in the Annapurna region can also be explained by a higher geothermal gradient. The optimal model from this inversion indeed shows a ramp dip that is closer to that inferred for the Langtang transect (21°) and a consequently somewhat higher (2°) detachment dip. However, this inversion favors a thermal structure that is even more extreme than that of LT1, with a best fit basal temperature of 1300°C and a stable near-surface geothermal gradient of 70°C km^{-1}. *Derry et al.* [2009] show that local hydrothermal gradients near hot springs located along the MCT in central Nepal reach 75°C km^{-1}, but these are strongly influenced by fluid advection and do not represent the overall geothermal gradient in the range. We expect the regional geothermal gradient to be closer to 30–35°C km^{-1} and therefore favor the result of AN1.

[44] Both inversions predict a MHT geometry for the Annapurna transect that is grossly similar to that of Langtang. Best fits impose the presence of a ramp below the MCT and physiographic transition. This ramp appears to be a bit steeper in west central Nepal than in east central Nepal.

[45] We use a similar inversion scheme to analyze the data from Bhutan (inversion BU1), with the final depth of the MHT at the northern boundary of the model as an additional free parameter (Figure 10). We choose to provide the inversion with this additional degree of freedom because there is no data to constrain the depth and geometry of the MHT in the Bhutan Himalaya. These models are fairly computationally intensive due to their size; we thus have to reduce the number of iterations. However, the NA inversion converges very rapidly to a solution. The BU1 inversion has the same set of parameters as AN2; since there is no indication in the AFT data of a possible out-of-sequence activation in Bhutan, we do not consider that possibility in the inversion. As expected from the very different pattern of AFT ages in Bhutan as compared to Nepal, the inversion results are completely different. In terms of thermal parameters, the inversion favors a relatively cool basal boundary condition ($T_0 = 716$°C) but a relatively high crustal heat production ($Q = 3.9$, corresponding to a depth-averaged heat production rate of 1.4 μW m^{-3}), leading to a stable near-surface geothermal gradient of 52°C km^{-1}. The contrast is strongest for the MHT geometry, as the optimal models favor a practically linear MHT, with a constant detachment dip of 5–7° from below the mountain front to the north edge of the model, where the MHT reaches ~42 km depth. Inversions with a lower imposed geothermal gradient (35°C km^{-1}) give similar results for the geometry of the MHT.

[46] These inversions thus clearly corroborate our initial qualitative interpretation of the different AFT age patterns: only subtle differences exist in the MHT geometry between western and eastern central Nepal, but a major difference exists between Nepal and Bhutan. In particular, the mid-crustal ramp disappears toward the east and the MHT becomes a planar detachment dipping 5–7° to the north.

5. Discussion

[47] Inversion results for the Langtang transect that aimed at testing the importance of recent out-of-sequence thrusting in the MCT zone are somewhat inconclusive. Sets of parameters can be found that allow both kinematic models to predict the data. However, we show that active out-of-sequence thrusting at the physiographic transition must have initiated recently (i.e., during the Quaternary) and requires either unrealistically high geothermal gradients or relatively rapid total overthrusting rates. The latter finding is consistent with inversion results presented by *Herman et al.* [2010], who used a similar approach. Moreover, significant out-of-sequence thrusting seems incompatible with the existence of a midcrustal ramp in the MHT. In contrast, models without Quaternary out-of-sequence thrusting require such a crustal ramp with a ~20° dip below this area. This latter geometry seems more compatible with the available reflection seismic profiles [*Hirn and Sapin*, 1984; *Zhao et al.*, 1993; *Makovsky et al.*, 1996; *Schulte-Pelkum et al.*, 2005; *Nabelek et al.*, 2009], as well as with seismicity data [*Pandey et al.*, 1999] and geoelectric soundings [*Lemonnier et al.*, 1999]. If out-of-sequence thrusting is active only during Quaternary times, the available AFT data from the Lesser Himalaya (where the greatest difference is predicted to occur; cf. Figure 5) do not have sufficient resolution to either corroborate or contradict it, because most AFT ages are ~5 Ma. As argued before, the younger AFT ages from the MCT zone cannot constrain the problem because the kinematic differences between the two models are subtle in the hanging wall of the proposed out-of-sequence thrust [e.g., *Whipp et al.*, 2007] (see Figure 5). Thus, the only possibility we envisage to obtain a clear answer to this question would be to obtain data recording the temperature history below the AFT closure temperature for the Lesser Himalaya, i.e., apatite fission track length distributions and/or (U-Th)/He data. Given our limited success in obtaining AFT ages from Lesser Himalayan rocks, the large amount of material required for meaningful length measurements in young samples and the quality criteria associated with apatite (U-Th)/He dating, we are pessimistic about the chances of success of such an undertaking.
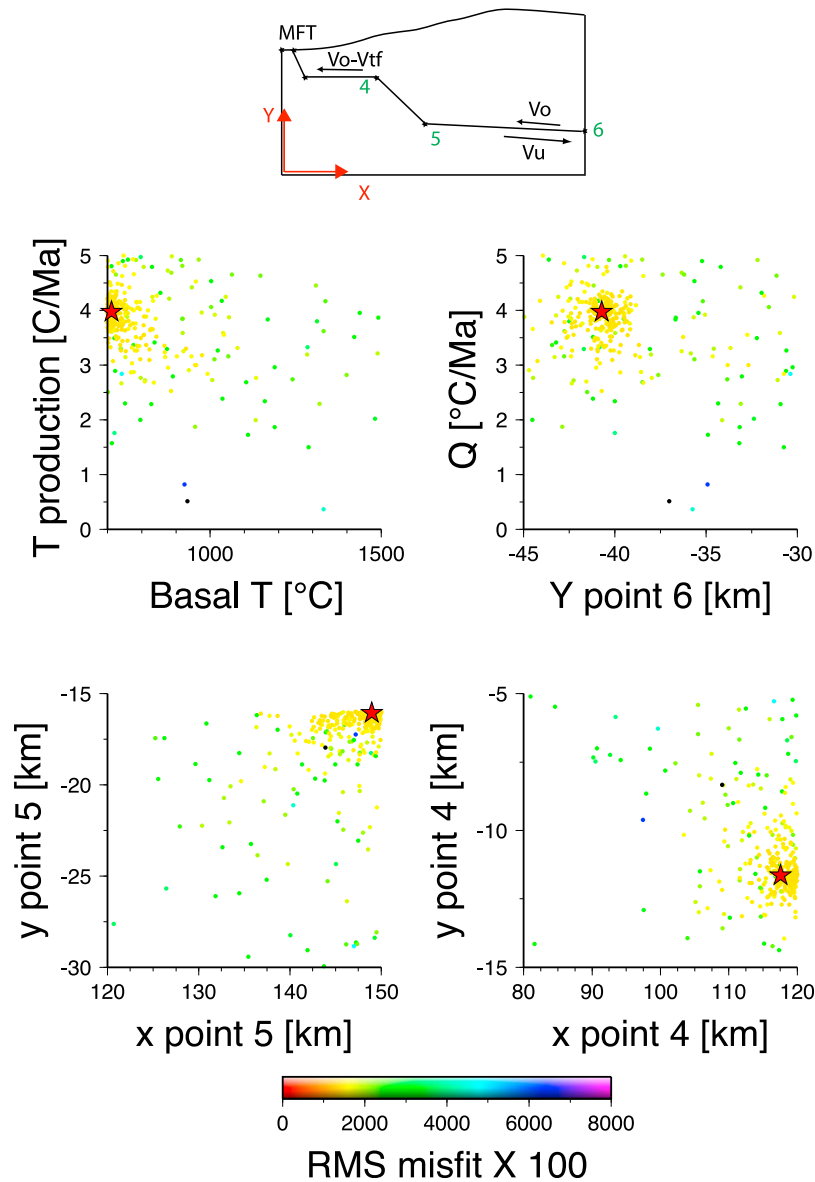
Figure 10. Scatter diagrams showing results of NA inversions for the Bhutan data. The sketch explains the significance of the free parameters controlling the geometry. Best fit is for a model with a planar MHT (no crustal ramp) dipping at 5–7°.

[48] The data do, however, constrain the geometry of the MHT and its lateral variations very well. Along-strike variations in thermochronological ages in the Himalaya are linked to along-strike variations in topography (Figures 2 and 3). Since the convergence velocity varies by <10% along strike and increases to the east, whereas exhumation rates decrease, these variations should be controlled by changes in kinematics associated with the geometry of the MHT. Where the MHT contains a midcrustal ramp, as in central Nepal, the flow of rocks over the ramp must be accompanied by high local relief with high exhumation and erosion rates in order to maintain steady state topography. The topographic profile will thus obtain a concave form. This is not necessary if the dip of the detachment is constant, leading to a linear to convex topographic surface and more constant exhumation rates across strike, and thus to a less

pronounced trend in thermochronological ages. These along-strike differences have previously been explained by an east-west climatic gradient [e.g., *Bookhagen and Burbank*, 2006; *Grujic et al.*, 2006]. However, in an active orogen with continuous convergence like the Himalaya, the transient response time to a climate shift should be less than a few My [e.g., *Whipple and Meade*, 2006] after which erosion rates are mainly controlled by the orogen kinematics. Our models do not include transient topography and therefore cannot address the potential effect on AFT ages of such shifts. However, *Herman et al.* [2010] did run models including an evolving topography and showed that the results were only subtly different from models with steady state topography.

[49] The Annapurna and Langtang transects show similar patterns in topography (Figure 2) and AFT ages (Figure 3),
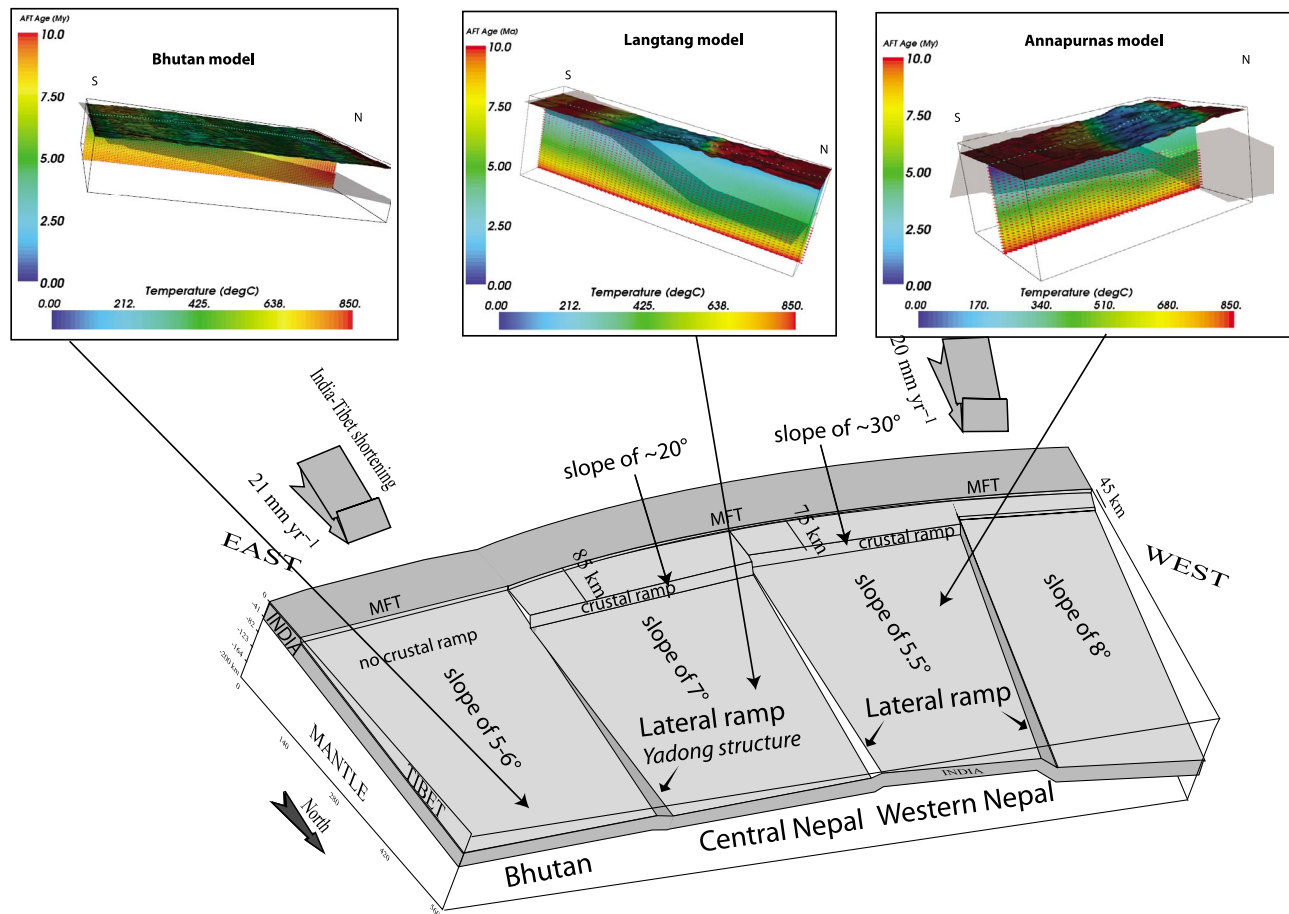
Figure 11. Schematic drawing showing 3-D view of MHT geometry and kinematics of the Himalaya from Nepal to Bhutan. Geometries of the best fit models from NA inversions are shown for comparison.

suggesting that both regions should be characterized by similar MHT geometry and kinematics. Our numerical models confirm this but suggest that the dip of the crustal ramp is somewhat steeper in the Annapurna area than in the Langtang area. Such a lateral variation of ramp dip is compatible with the conclusions of *Berger et al.* [2004], who inferred lateral variations in the geometry of the MHT in Nepal from the analysis of present-day (GPS derived) displacement rates. They propose the existence of lateral ramps to permit the transition between areas with different crustal ramp dips. In particular, they show that in western-most Nepal, the midcrustal ramp should be much less well expressed and the shallow detachment dip more important than in central Nepal, in agreement with inferences from drainage patterns [*van der Beek et al.*, 2002]. The topographic transition between the Lesser and High Himalaya also becomes less well expressed in western Nepal [*Berger et al.*, 2004]. Sampling a thermochronological age transect across the Lesser and the Higher Himalaya in western Nepal could test our model, which predicts that minimum AFT ages in the MCT zone should be older than in central Nepal and the increase in ages toward the south less pronounced, if existent at all.

[50] AFT data show that exhumation rates in the MCT zone and the topographically highest part of the range are lower in Bhutan than in Nepal. This is consistent with

observations of the regional geology of the Himalaya. In western and central Bhutan, the Higher Himalaya is much more widespread than in central Nepal, to the expense of the Lesser Himalaya (cf. Figure 1). As clearly shown by the Higher Himalayan klippen in Nepal, the Higher Himalayan sequence has overthrusted the Lesser Himalaya on a nearly horizontal detachment [e.g., *Schelling and Arita*, 1991; *Upreti and Le Fort*, 1999; *DeCelles et al.*, 2001]. We can thus interpret the regional variation in surface geology as a consequence of a variation in the depth of erosion between the central and eastern Himalaya. As GPS measurements show a somewhat higher convergence rate in the eastern Himalaya compared to the western Himalaya, the sole solution to allow coexistent higher convergence rates and lower exhumation rates is to reduce the angle of the MHT detachment.

[51] Our interpretation and numerical modeling of the lateral variations in AFT age patterns permit us to present a conceptual 3D view of the MHT below Nepal and Bhutan (Figure 11). The geometry of the MHT is clearly not laterally constant. In western Nepal, the southern shallow flat of the MHT is steeper than in central Nepal [*Larson et al.*, 1999; *van der Beek et al.*, 2002], but the dip angle of the midcrustal MHT ramp is steeper in central Nepal than in western Nepal [*Berger et al.*, 2004]. Within the central Nepal segment, more subtle variations appear to exist

between the Annapurna and Langtang regions, as implied by our inversions, but we cannot definitely state at this stage whether these differences are real or beyond the resolution of our model. In Bhutan, the MHT appears as a continuous shallowly dipping detachment without a ramp below our model domain. If a midcrustal ramp exists below the eastern Himalaya it should be located more to the north, possibly associated with exhumation of the Kangmar dome in southern Tibet, as suggested by *Hauck et al.* [1998]. This interpretation implies important and fairly rapid changes of geometry between each zone (western Nepal, central Nepal and Bhutan), most easily explained by the presence of lateral crustal ramps within the underthrusting Indian crust. *Hauck et al.* [1998] suggest that the Yadong Cross structure in westernmost Bhutan represents one of these lateral ramps and controls the transition zone between the Bhutan and Nepal Himalaya [see also *Duncan et al.*, 2003].

[52] Our analysis thus poses the question of what is the fundamental control on topography in the Himalaya and in collisional mountain belts in general. *Bookhagen et al.* [2005], *Bookhagen and Burbank* [2006], and *Grujic et al.* [2006] have argued for a strong climatic control on laterally varying topographic trends, due to the lateral variations in precipitation rates and patterns observed in the Himalaya. We show, however, that lateral variations in topography and exhumation rates should also be correlated to variations in the geometry of the MHT and associated crustal kinematics. Our study underlines the strong influence of the geometry of deep tectonic structures on the topography of mountain belts. Increasing relief will lead to enhanced erosion through the relief dependence of major erosional mechanisms [e.g., *Montgomery and Brandon*, 2002]. Increasing elevation also leads to higher erosion rates by orographic enhancement of precipitation rates [e.g., *Roe*, 2005]. Thus, our study highlights the complex couplings in the system but emphasizes the potentially important role of preexisting structure, which may have been somewhat overlooked in recent years. In this respect, our study supports the findings of *Burbank et al.* [2003], who suggested that the pattern of exhumation rates across the central Nepal Himalaya is strongly controlled by the underlying crustal kinematics and only weakly influenced by present-day precipitation patterns.

6. Conclusions

[53] Low-temperature thermochronology data from the Lesser Himalaya in central Nepal currently lack the resolution to assess the importance of Quaternary out-of-sequence faulting at the physiographic transition. However, the geometry of the MHT required by a model in which overthrusting is concentrated on the MHT and the frontal thrust appears more consistent with available geophysical data than that for models with significant out-of-sequence thrusting. Out-of-sequence thrusting thus appears to be a secondary mechanism at best for explaining the observed pattern of thermochronological ages in comparison to the geometry of main crustal faults.

[54] The tectonic structure and geomorphology of the Himalaya clearly show that the structure of the orogen is not laterally uniform. We link along-strike variations in topography and exhumation patterns to the geometry of crustal-scale faults. These faults and their associated kinematics

control topography through the uplift and exhumation pathways of rocks. The presence of a midcrustal ramp in central Nepal induces the formation of a sharp topographic transition, whereas both the midcrustal ramp and the topographic transition are absent in the Bhutan Himalaya. The formation of relief strongly influences precipitation and erosion rates, and explains the gradient of denudation from west to east, underlined by variations in map view of the outcrop pattern of the Higher and Lesser Himalaya. This study therefore underlines the importance of inherited crustal-scale geometry and associated kinematics in driving topography and exhumation.

References

Adams, J. (1980), Contemporary uplift and erosion of the Southern Alps, New Zealand, *Geol. Soc. Am. Bull.*, *91*, 2–4, doi:10.1130/0016-7606 (1980)91<2:CUAEOT>2.0.CO;2.

Anders, A. M., G. H. Roe, B. Hallet, D. R. Montgomery, N. J. Finnegan, and J. Putkonen (2006), Spatial patterns of precipitation and topography in the Himalaya, in *Tectonics, Climate, and Landscape Evolution*, edited by S. D. Willett et al., *Spec. Pap. Geol. Soc. Am.*, *398*, 39–53.

Arita, K., R. D. Dallmeyer, and A. Takasu (1997), Tectonothermal evolution of the Lesser Himalaya, Nepal: Constraints from ^{40}Ar/^{39}Ar ages from the Kathmandu Nappe, *Island Arc*, *6*, 372–385, doi:10.1111/ j.1440-1738.1997.tb00047.x.

Avouac, J. P. (2003), Mountain building, erosion and the seismic cycle in the Nepal Himalaya, *Adv. Geophys.*, *46*, 1–80, doi:10.1016/S0065-2687(03) 46001-9.

Batt, G. E., and J. Braun (1997), On the thermo-mechanical evolution of compressional orogens, *Geophys. J. Int.*, *128*, 364–382, doi:10.1111/ j.1365-246X.1997.tb01561.x.

Beaumont, C., R. A. Jamieson, M. H. Nguyen, and B. Lee (2001), Himalayan tectonics explained by extrusion of a low-viscosity channel coupled to focused surface denudation, *Nature*, *414*, 738–742, doi:10.1038/414738a.

Berger, A., F. Jouanne, R. Hassani, and J. L. Mugnier (2004), Modelling the spatial distribution of present-day deformation in Nepal: How cylindrical is the Main Himalayan Thrust in Nepal?, *Geophys. J. Int.*, *156*, 94–114, doi:10.1111/j.1365-246X.2004.02038.x.

Bhargava, O. N. (1995), Geology of Bhutan: A synoptic view, in *The Bhutan Himalaya: A Geological Account*, edited by O. N. Bhargava, *Spec. Publ. Geol. Soc. India*, 39, 13–17.

Bilham, R., K. Larson, and J. Freymueller, and the Project IDYLHIM Members (1997), GPS measurements of present-day convergence across the Nepal Himalaya, *Nature*, *386*, 61–64, doi:10.1038/386061a0.

Blythe, A., D. W. Burbank, A. Carter, K. L. Schmidt, and J. Putkonen (2007), Plio-Quaternary exhumation history of the central Himalaya: 1. Apatite and zircon fission track and apatite [U-Th]/He analyses, *Tectonics*, *26*, TC3002, doi:10.1029/2006TC001990.

Bollinger, L., J.-P. Avouac, E. J. Catlos, T. M. Harrison, M. Grove, O. Beyssac, B. Goffé, and S. Sapkota (2004), Thermal structure and exhumation history of the Lesser Himalaya in central Nepal, *Tectonics*, *23*, TC5015, doi:10.1029/2003TC001564.

Bollinger, L., P. Henry, and J. P. Avouac (2006), Mountain building in the Nepal Himalaya: Thermal and kinematic model, *Earth Planet. Sci. Lett.*, *244*, 58–71, doi:10.1016/j.epsl.2006.01.045.

Bookhagen, B., and D. W. Burbank (2006), Topography, relief, and TRMM-derived rainfall variations along the Himalaya, *Geophys. Res. Lett.*, *33*, L08405, doi:10.1029/2006GL026037.

Bookhagen, B., R. C. Thiede, and M. R. Strecker (2005), Abnormal monsoon years and their control on erosion and sediment flux in the high, arid northwest Himalaya, *Earth Planet. Sci. Lett.*, *231*, 131–146, doi:10.1016/j.epsl.2004.11.014.

Braun, J. (2002), Quantifying the effect of recent relief changes on age-elevation relationships, *Earth Planet. Sci. Lett.*, *200*, 331–343, doi:10.1016/S0012-821X(02)00638-6.

Braun, J. (2003), Pecube: A new finite element code to solve the heat transport equation in three dimensions in the Earth's crust including the effects of a time-varying, finite amplitude surface topography, *Comput. Geosci.*, *29*, 787–794, doi:10.1016/S0098-3004(03)00052-9.

Braun, J., and X. Robert (2005), Constraints on the rate of post-orogenic erosional decay from low-temperature thermochronological data: Application to the Dabie Shan, China, *Earth Surf. Processes Landforms*, *30*, 1203–1225, doi:10.1002/esp.1271.

Braun, J., G. E. Batt, D. L. Scott, H. McQueen, and A. R. Beasley (1994), A simple kinematic model for crustal deformation along two- and three-dimensional listric normal faults derived from scaled laboratory experiments, *J. Struct. Geol.*, *16*, 1477–1490, doi:10.1016/0191-8141(94)90010-8.

Braun, J., P. van der Beek, and G. Batt (2006), *Quantitative Thermochronology: Numerical Methods for the Interpretation of Thermochronological Data*, 258 pp., Cambridge Univ. Press, New York, doi:10.1017/CBO9780511616433.

Brewer, I. D., and D. W. Burbank (2006), Thermal and kinematic modeling of bedrock and detrital cooling ages in the central Himalaya, *J. Geophys. Res.*, *111*, B09409, doi:10.1029/2004JB003304.

Brunel, M., and J. Andrieux (1980), Sur un modèle explicatif du métamorphisme inverse himalayen, *C. R. Acad. Sci.*, *291*, 609–612.

Burbank, D. W. (2002), Rates of erosion and their implications for denudation, *Mineral. Mag.*, *66*, 25–52, doi:10.1180/0026461026610014.

Burbank, D. W., A. E. Blythe, J. K. Putkonen, B. A. Pratt-Sitaula, E. J. Gabet, M. E. Oskin, A. P. Barros, and T. P. Ojha (2003), Decoupling of erosion and precipitation in the Himalaya, *Nature*, *426*, 652–655, doi:10.1038/nature02187.

Burchfiel, B. C., C. Zhiliang, K. V. Hodges, L. Yuping, L. H. Royden, D. Changrong, and X. Jiene (1992), The South Tibetan detachment system, Himalayan orogen: Extension contemporaneous with and parallel to shortening in a collisional mountain belt, *Spec. Pap. Geol. Soc. Am.*, *269*, 41 pp.

Catlos, E. J., T. M. Harrison, M. J. Kohn, M. Grove, F. J. Ryerson, C. E. Manning, and B. N. Upreti (2001), Geochronologic and barometric constraints on the evolution of the Main Central Thrust, central Nepal Himalaya, *J. Geophys. Res.*, *106*, 16,177–16,204, doi:10.1029/2000JB900375.

Cattin, E., and J. P. Avouac (2000), Modeling mountain building and the seismic cycle in the Himalaya of Nepal, *J. Geophys. Res.*, *105*, 13,389–13,407, doi:10.1029/2000JB900032.

Copeland, P., T. M. Harisson, K. V. Hodges, P. Maruejol, P. Le Fort, and A. Pêcher (1991), An Early Pliocene thermal disturbance of the Main Central Thrust, central Nepal: Implications for Himalayan tectonics, *J. Geophys. Res.*, *96*, 8475–8500, doi:10.1029/91JB00178.

DeCelles, P. G., G. E. Gehrels, J. Quade, T. P. Ojha, P. A. Kapp, and B. N. Upreti (1998), Neogene foreland basin deposits, erosional unroofing, and the kinematic history of the Himalayan fold-thrust belt, western Nepal, *Geol. Soc. Am. Bull.*, *110*, 2–21, doi:10.1130/0016-7606(1998)110<0002:NFBDEU>2.3.CO;2.

DeCelles, P. G., G. E. Gehrels, J. Quade, B. LaReau, and M. Spurlin (2000), Tectonic implications of U-Pb zircon ages of the Himalayan orogenic belt in Nepal, *Science*, *288*, 497–499, doi:10.1126/science.288.5465.497.

DeCelles, P. G., D. M. Robinson, J. Quade, T. P. Ojha, C. N. Garzione, P. Copeland, and B. N. Upreti (2001), Stratigraphy, structure, and tectonic evolution of the Himalayan fold-thrust belt in western Nepal, *Tectonics*, *20*, 487–509, doi:10.1029/2000TC001226.

Derry, L. A., M. J. Evans, R. Darling, and C. France-Lanord (2009), Hydrothermal heat flow near the Main Central Thrust, central Nepal Himalaya, *Earth Planet. Sci. Lett.*, *286*, 101–109, doi:10.1016/j.epsl.2009.06.036.

Duncan, C., J. Masek, and E. Fielding (2003), How steep are the Himalaya? Characteristics and implications of along-strike topographic variations, *Geology*, *31*, 75–78, doi:10.1130/0091-7613(2003)031<0075:HSATHC>2.0.CO;2.

Ehlers, T. A. (2005), Crustal thermal processes and thermochronometer interpretation, in *Low-temperature Thermochronology: Techniques, Interpretations, and Applications*, vol. 58, edited by P. W. Reiners and T. A. Ehlers, pp. 315–350, Mineral. Soc. of Am., Chantilly, Va.

Galbraith, R. F., and G. M. Laslett (1993), Statistical models for mixed fission track ages, *Nucl. Tracks Radiat. Meas.*, *21*, 459–470, doi:10.1016/1359-0189(93)90185-C.

Galy, V., C. France-Lanord, B. Peucker-Ehrenbrink, and P. Huyghe (2010), Sr-Nd-Os evidence for a stable erosion regime in the Himalaya during the past 12 Myr, *Earth Planet. Sci. Lett.*, *290*, 474–480, doi:10.1016/j.epsl.2010.01.004.

Gansser, A. (1964), *Geology of the Himalayas*, 289 pp., John Wiley, London.

Gansser, A. (1983), *Geology of the Bhutan Himalaya*, 181 pp., Birkhaeuser, Basel, Switzerland.

Gehrels, G. E., P. G. DeCelles, T. P. Ojha, and B. N. Upreti (2006), Geologic and U-Th-Pb geochronologic evidence for early Paleozoic tectonism in the Kathmandu thrust sheet, central Nepal Himalaya, *Geol. Soc. Am. Bull.*, *118*, 185–198, doi:10.1130/B25753.1.

Green, P. F., I. R. Duddy, G. M. Laslett, K. A. Hegarty, A. J. W. Gleadow, and J. F. Lovering (1989), Thermal annealing of fission tracks in apatite 4. Quantitative modelling techniques and extension to geological time-scales, *Chem. Geol.*, *79*, 155–182, doi:10.1016/0168-9622(89)90018-3.

Grujic, D., L. S. Hollister, and R. R. Parrish (2002), Himalayan metamorphic sequence as an orogenic channel: Insight from Bhutan, *Earth Planet. Sci. Lett.*, *198*, 177–191, doi:10.1016/S0012-821X(02)00482-X.

Grujic, D., I. Coutand, B. Bookhagen, S. Bonnet, A. Blythe, and C. Duncan (2006), Climatic forcing of erosion, landscape, and tectonics in the Bhutan Himalayas, *Geology*, *34*, 801–804, doi:10.1130/G22648.1.

Harrison, T. M., M. Grove, O. M. Lovera, and E. J. Catlos (1998), A model for the origin of the Himalayan anatexis and inverted metamorphism, *J. Geophys. Res.*, *103*, 27,017–27,032, doi:10.1029/98JB02468.

Hauck, M. L., K. D. Nelson, L. D. Brown, W. Zhao, and A. R. Ross (1998), Crustal structure of the Himalayan orogen at ~90° east longitude from Project INDEPTH deep reflection profiles, *Tectonics*, *17*, 481–500, doi:10.1029/98TC01314.

Herman, F., et al. (2010), Exhumation, crustal deformation, and thermal structure of the Nepal Himalaya derived from the inversion of thermochronological and thermobarometric data and modeling of the topography, *J. Geophys. Res.*, *115*, B06407, doi:10.1029/2008JB006126.

Hirn, A., and M. Sapin (1984), The Himalayan zone of crustal interaction: Suggestions from explosion seismology, *Ann. Geophys.*, *2*, 123–130.

Hodges, K. V. (2000), Tectonics of the Himalaya and southern Tibet from two perspectives, *Geol. Soc. Am. Bull.*, *112*, 324–350, doi:10.1130/0016-7606(2000)112<324:TOTHAS>2.0.CO;2.

Hodges, K. V., R. R. Parrish, and M. P. Searle (1996), Tectonic evolution of the central Annapurna Range, Nepalese Himalayas, *Tectonics*, *15*, 1264–1291, doi:10.1029/96TC01791.

Hodges, K. V., J. M. Hurtado, and K. X. Whipple (2001), Southward extrusion of Tibetan crust and its effect on Himalayan tectonics, *Tectonics*, *20*, 799–809, doi:10.1029/2001TC001281.

Hodges, K. V., C. W. Wobus, K. Ruhl, T. Schildgen, and K. X. Whipple (2004), Quaternary deformation, river steepening, and heavy precipitation at the front of the Higher Himalayan ranges, *Earth Planet. Sci. Lett.*, *220*, 379–389, doi:10.1016/S0012-821X(04)00063-9.

Hollister, L. S., and D. Grujic (2006), Pulsed channel flow in Bhutan, in *Channel Flow, Ductile Extrusion and Exhumation in Continental Collision Zones*, edited by R. D. Law et al., *Geol. Soc. Spec. Publ.*, *268*, 415–423.

Hovius, N. (1998), Controls on sediment supply by large rivers, in *Relative Role of Eustacy, Climate and Tectonics in Continental Rocks*, edited by K. W. Shanley and P. J. McCabe, *Spec. Publ. Soc. Econ. Paleontol. Mineralogists.*, *59*, 3–16.

Huntington, K. W., T. A. Ehlers, K. V. Hodges, and D. M. Whipp Jr. (2007), Topography, exhumation pathway, age uncertainties, and the interpretation of thermochronometer data, *Tectonics*, *26*, TC4012, doi:10.1029/2007TC002108.

Huyghe, P., A. Galy, J. L. Mugnier, and C. France-Lanord (2001), Propagation of the thrust system and erosion in the Lesser Himalaya: Geochemical and sedimentological evidence, *Geology*, *29*, 1007–1010, doi:10.1130/0091-7613(2001)029<1007:POTTSA>2.0.CO;2.

Jamieson, R. A., and C. Beaumont (1988), Orogeny and metamorphism: A model for deformation and pressure-temperature-time paths with applications to the central and southern Appalachians, *Tectonics*, *7*, 417–445, doi:10.1029/TC007i003p00417.

Jouanne, F., J. L. Mugnier, J. F. Gamond, P. Le Fort, M. R. Pandey, L. Bollinger, M. Flouzat, and J. P. Avouac (2004), Current shortening across the Himalayas of Nepal, *Geophys. J. Int.*, *157*, 1–14, doi:10.1111/j.1365-246X.2004.02180.x.

Lakshminarayana, G., and B. Singh (1995), Siwalik group, in *The Bhutan Himalaya: A Geological Account*, edited by O. N. Bhargava, *Spec. Publ. Geol. Soc. India*, 39, 22–28.

Larson, K. M., R. Bürgmann, R. Bilham, and J. T. Freymueller (1999), Kinematics of the India-Eurasia collision zone from GPS measurements, *J. Geophys. Res.*, *104*, 1077–1093, doi:10.1029/1998JB900043.

Lavé, J., and J. P. Avouac (2000), Active folding of fluvial terraces across the Siwaliks Hills (Himalayas of central Nepal), *J. Geophys. Res.*, *105*, 5735–5770, doi:10.1029/1999JB900292.

Lavé, J., and J. P. Avouac (2001), Fluvial incision and tectonic uplift across the Himalayas of central Nepal, *J. Geophys. Res.*, *106*, 26,561–26,591, doi:10.1029/2001JB000359.

Le Fort, P. (1975), Himalaya: The collided range. Present knowledge of the continental arc, *Am. J. Sci.*, *275*, 1–44.

Lemonnier, C., G. Marquis, F. Perrier, J.-P. Avouac, G. Chitrakar, B. Kafle, S. Sapkota, U. Gautam, D. Tiwari, and M. Bano (1999), Electrical structure of the Himalaya of central Nepal: High conductivity around the mid-crustal ramp along the MHT, *Geophys. Res. Lett.*, *26*, 3261–3264, doi:10.1029/1999GL008363.

Makovsky, Y., S. L. Klemperer, H. Liyan, and L. Deyuan, and the Project INDEPTH Team (1996), Structural elements of the southern Tethyan Himalaya crust from wide-angle seismic data, *Tectonics*, *15*, 997–1005, doi:10.1029/96TC00310.

Mancktelow, N. S., and B. Grasemann (1997), Time-dependent effects of heat advection and topography on cooling histories during erosion, *Tectonophysics*, *270*, 167–195, doi:10.1016/S0040-1951(96)00279-X.

McQuarrie, N., D. Robinson, S. Long, T. Tobgay, D. Grujic, G. Gehrels, and M. Ducea (2008), Preliminary stratigraphic and structural architecture of Bhutan: Implications for the along strike architecture of the Himalayan system, *Earth Planet. Sci. Lett.*, *272*, 105–117, doi:10.1016/j.epsl.2008.04.030.

Meigs, A. J., D. W. Burbank, and R. A. Beck (1995), Middle-Late Miocene (>10 Ma) formation of the Main Boundary Thrust in the western Himalaya, *Geology*, *23*, 423–426, doi:10.1130/0091-7613(1995)023<0423:MLMMFO>2.3.CO;2.

Montgomery, D. R., and M. T. Brandon (2002), Topographic controls on erosion rates in tectonically active mountain ranges, *Earth Planet. Sci. Lett.*, *201*, 481–489, doi:10.1016/S0012-821X(02)00725-2.

Mugnier, J.-L., and P. Huyghe (2006), Ganges basin geometry records a pre-15 Ma isostatic rebound of Himalaya, *Geology*, *34*, 445–448, doi:10.1130/G22089.1.

Mugnier, J. L., P. Leturmy, G. Mascle, P. Huyghe, E. Chalaron, G. Vidal, L. Husson, and B. Delcaillau (1999), The Siwaliks of western Nepal: I - Geometry and kinematics, *J. Asian Earth Sci.*, *17*, 629–642, doi:10.1016/S1367-9120(99)00038-3.

Mugnier, J., P. Huyghe, P. Leturmy, and F. Jouanne (2004), Episodicity and rates of thrust sheet motion in the Himalayas (western Nepal), in *Thrust Tectonics and Petroleum Systems*, edited by K. C. McClay, *AAPG Mem.*, *82*, 1–24.

Nabelek, J., G. Hetenyi, J. Vergne, S. Sapkota, B. Kafle, M. Jiang, H. Su, J. Chen, and B.-S. Huang, and the Hi-CLIMB Team (2009), Underplating in the Himalaya-Tibet collision zone revealed by the Hi-CLIMB experiment, *Science*, *325*, 1371–1374, doi:10.1126/science.1167719.

Nelson, K. D., et al. (1996), Partially molten middle crust beneath southern Tibet: Synthesis of project INDEPTH results, *Science*, *274*, 1684–1688, doi:10.1126/science.274.5293.1684.

Pandey, M. R., R. P. Tandukar, J. P. Avouac, J. Vergne, and T. Héritier (1999), Seismotectonics of the Nepal Himalaya from a local seismic network, *J. Asian Earth Sci.*, *17*, 703–712, doi:10.1016/S1367-9120(99)00034-6.

Paul, J., et al. (2001), The motion and active deformation of India, *Geophys. Res. Lett.*, *28*, 647–650, doi:10.1029/2000GL011832.

Pearson, O. N., and P. G. DeCelles (2005), Structural geology and regional tectonic significance of the Ramgarh thrust, Himalayan fold-thrust belt of Nepal, *Tectonics*, *24*, TC4008, doi:10.1029/2003TC001617.

Powers, P. M., R. J. Lillie, and R. S. Yeats (1998), Structure and shortening of the Kangra and Dehra Dun reentrants, sub-Himalaya, India, *Geol. Soc. Am. Bull.*, *110*, 1010–1027, doi:10.1130/0016-7606(1998)110<1010:SASOTK>2.3.CO;2.

Rai, S. M. (1998), Les Nappes de Kathmandou et du Gosainkund, Himalaya du Népal central (Etude cartographique, structurale, métamorphique, géochimique et radiochronologique), Ph.D. thesis, 150 pp, Univ. Joseph Fourier, Grenoble, France.

Reiners, P. W., and M. T. Brandon (2006), Using thermochronology to understand orogenic erosion, *Annu. Rev. Earth Planet. Sci.*, *34*, 419–466, doi:10.1146/annurev.earth.34.031405.125202.

Robert, X., P. van der Beek, J. Braun, J.-L. Mugnier, C. Perry, and M. Dubille (2009), Assessing Quaternary reactivation of the Main Central Thrust zone (central Nepal Himalaya): New thermochronologic data and numerical modelling, *Geology*, *37*, 731–734, doi:10.1130/G25736A.1.

Robinson, D. M., P. G. DeCelles, and P. Copeland (2006), Tectonic evolution of the Himalayan thrust belt in western Nepal: Implications for channel flow models, *Geol. Soc. Am. Bull.*, *118*, 865–885, doi:10.1130/B25911.1.

Roe, G. H. (2005), Orographic precipitation, *Annu. Rev. Earth Planet. Sci.*, *33*, 645–671, doi:10.1146/annurev.earth.33.092203.122541.

Sambridge, M. (1999a), Geophysical inversion with a neighbourhood algorithm - I. Searching a parameter space, *Geophys. J. Int.*, *138*, 479–494, doi:10.1046/j.1365-246X.1999.00876.x.

Sambridge, M. (1999b), Geophysical inversion with a neighbourhood algorithm - II. Appraising the ensemble, *Geophys. J. Int.*, *138*, 727–746, doi:10.1046/j.1365-246x.1999.00900.x.

Schelling, D., and K. Arita (1991), Thrust tectonics, crustal shortening, and the structure of the far eastern Nepal Himalaya, *Tectonics*, *10*, 851–862, doi:10.1029/91TC01011.

Schulte-Pelkum, V., G. Monsalve, A. Sheehan, M. R. Pandey, S. Sapkota, R. Bilham, and F. Wu (2005), Imaging the Indian subcontinent beneath the Himalaya, *Nature*, *435*, 1222–1225, doi:10.1038/nature03678.

Seeber, L., and V. Gornitz (1983), River profiles along the Himalayan arc as indicators of active tectonics, *Tectonophysics*, *92*, 335–367, doi:10.1016/0040-1951(83)90201-9.

Srivastava, P., and G. Mitra (1994), Thrust geometries and deep structure of the outer and Lesser Himalaya, Kumaon and Garhwal (India): Implications for evolution of the Himalayan fold- and-thrust belt, *Tectonics*, *13*, 89–110, doi:10.1029/93TC01130.

Stephenson, J., K. Gallagher, and C. C. Holmes (2006), A Bayesian approach to calibrating apatite fission track annealing models for laboratory and geological timescales, *Geochim. Cosmochim. Acta*, *70*, 5183–5200, doi:10.1016/j.gca.2006.07.027.

Stolar, D. B., G. H. Roe, and S. D. Willett (2007), Controls on the patterns of topography and erosion rate in a critical orogen, *J. Geophys. Res.*, *112*, F04002, doi:10.1029/2006JF000713.

Stüwe, K., L. White, and R. W. Brown (1994), The influence of eroding topography on steady-state isotherms: Application to fission track analysis, *Earth Planet. Sci. Lett.*, *124*, 63–74, doi:10.1016/0012-821X(94)00068-9.

Summerfield, M. A., and N. J. Hulton (1994), Natural controls of fluvial denudation rates in major world drainage basins, *J. Geophys. Res.*, *99*, 13,871–13,883, doi:10.1029/94JB00715.

Thiede, R. C., B. Bookhagen, J. R. Arrowsmith, E. R. Sobel, and M. R. Strecker (2004), Climatic control on rapid exhumation along the Southern Himalayan Front, *Earth Planet. Sci. Lett.*, *222*, 791–806, doi:10.1016/j.epsl.2004.03.015.

Upreti, B. N. (1999), An overview of the stratigraphy and tectonics of the Nepal Himalaya, *J. Asian Earth Sci.*, *17*, 577–606, doi:10.1016/S1367-9120(99)00047-4.

Upreti, B. N., and P. Le Fort (1999), Lesser Himalayan crystalline nappes of Nepal: Problems of their origin, in *Himalaya and Tibet: Mountain Roots to Mountain Tops*, edited by A. MacFarlane et al., *Spec. Pap. Geol. Soc. Am.*, *328*, 225–238.

Valla, P. G., F. Herman, P. A. van der Beek, and J. Braun (2010), Inversion of thermochronological age-elevation profiles to extract independent estimates of denudation and relief history - I: Theory and conceptual model, *Earth Planet. Sci. Lett.*, *295*, 511–522, doi:10.1016/j.epsl.2010.04.033.

van der Beek, P. A., B. Champel, and J. L. Mugnier (2002), Control of detachment dip on drainage development in regions of active fault-propagation folding, *Geology*, *30*, 471–474, doi:10.1130/0091-7613(2002)030<0471:CODDOD>2.0.CO;2.

van der Beek, P. A., X. Robert, J. L. Mugnier, M. Bernet, P. Huyghe, and E. Labrin (2006), Late Miocene-Recent exhumation of the central Himalaya and recycling in the foreland basin assessed by apatite fission track thermochronology of Siwalik sediments, Nepal, *Basin Res.*, *18*, 413–434, doi:10.1111/j.1365-2117.2006.00305.x.

Vannay, J.-C., B. Grasemann, M. Rahn, W. Frank, A. Carter, V. Baudraz, and M. Cosca (2004), Miocene to Holocene exhumation of metamorphic crustal wedges in the NW Himalaya: Evidence for tectonic extrusion coupled to fluvial erosion, *Tectonics*, *23*, TC1014, doi:10.1029/2002TC001429.

Whipp, D. M., T. A. Ehlers, A. Blythe, K. W. Huntington, K. V. Hodges, and D. W. Burbank (2007), Plio-Quaternary exhumation history of the central Nepalese Himalaya: 2. Thermokinematic and thermochronometer age prediction model, *Tectonics*, *26*, TC3003, doi:10.1029/2006TC001991.

Whipple, K. X., and B. J. Meade (2006), Orogen response to changes in climatic and tectonic forcing, *Earth Planet. Sci. Lett.*, *243*, 218–228, doi:10.1016/j.epsl.2005.12.022.

Willett, S. D. (1999), Orogeny and orography: The effects of erosion on the structure of mountain belts, *J. Geophys. Res.*, *104*, 28,957–28,981, doi:10.1029/1999JB900248.

Willett, S. D., and M. T. Brandon (2002), On steady state in mountain belts, *Geology*, *30*, 175–178, doi:10.1130/0091-7613(2002)030<0175: OSSIMB>2.0.CO;2.

Wobus, C. W., K. V. Hodges, and K. X. Whipple (2003), Has focused denudation sustained active thrusting at the Himalayan topographic front?, *Geology*, *31*, 861–864, doi:10.1130/G19730.1.

Wobus, C. W., A. Heimsath, K. X. Whipple, and K. V. Hodges (2005), Active out-of-sequence thrust faulting in the central Nepalese Himalaya, *Nature*, *434*, 1008–1011, doi:10.1038/nature03499.

Wobus, C. W., K. X. Whipple, and K. V. Hodges (2006), Neotectonics of the central Nepalese Himalaya: Constraints from geomorphology, detrital ^{40}Ar/^{39}Ar thermochronology, and thermal modeling, *Tectonics*, *25*, TC4011, doi:10.1029/2005TC001935.

Yin, A. (2006), Cenozoic tectonic evolution of the Himalayan orogen as constrained by along-strike variation of structural geometry, exhumation history, and foreland sedimentation, *Earth Sci. Rev.*, *76*, 1–131, doi:10.1016/j.earscirev.2005.05.004.

Yin, A., and T. M. Harrison (2000), Geologic evolution of the Himalayan-Tibetan orogen, *Annu. Rev. Earth Planet. Sci.*, *28*, 211–280, doi:10.1146/annurev.earth.28.1.211.

Zhao, W., K. D. Nelson, and the Project INDEPTH Team (1993), Deep seismic reflection evidence for continental underthrusting beneath southern Tibet, *Nature*, *366*, 557–559, doi:10.1038/366557a0.

J. Braun and P. van der Beek, Institut des Sciences de la Terre, Université Joseph Fourier, CNRS, BP 53, F-38041 Grenoble, France.

J.-L. Mugnier, Institut des Sciences de la Terre, CNRS, Université de Savoie, F-73376 Le Bourget-du-Lac, CEDEX, France.

C. Perry and X. Robert, GEOTOP, Département des Sciences de la Terre et de L'atmosphère, Université du Québec à Montréal, Montreal, QC H3C 3P8, Canada. (xavier.robert01@gmail.com)